Article:
Ibn-Mohammed, T. orcid.org/0000-0003-2454-0303, Koh, S.C.L., Mustapha, K.B. et al. (8 more authors) (2023) Techno-environmental analysis of material substitution in thermoelectric modules: non-oxide (bismuth telluride alloys) vs. oxide-based (lanthanum-doped strontium titanate and calcium cobaltite) materials. Energy Conversion and Management: X, 19. 100395. ISSN 2590-1745

https://doi.org/10.1016/j.ecmx.2023.100395

Energy Conversion and Management: X 19 (2023) 100395

Contents lists available at ScienceDirect

Energy Conversion and Management: X

journal homepage: www.sciencedirect.com/journal/energy-conversion-and-management-x

Techno-environmental analysis of material substitution in thermoelectric modules: non-oxide (bismuth telluride alloys) vs. oxide-based (lanthanum-doped strontium titanate and calcium cobaltite) materials

T. Ibn-Mohammed [a,*], S.C.L. Koh [b,c], K.B. Mustapha [d], L. Smith [b,e,g], A. Acquaye [f], A.C. Iyasara [g], F. Hussain [h], N. Morley [g], D.C. Sinclair [g], C.A. Randall [i], I.M. Reaney [c,g,1]

[a] Computational Sustainability Research Group (CSRG), WMG, The University of Warwick, Coventry, CV4 7AL, UK
[b] Advanced Resource Efficiency Centre (AREC), The University of Sheffield, Sheffield, S10 1FL, UK
[c] Energy Institute, The University of Sheffield, Sheffield S10 1FL, UK
[d] Faculty of Engineering & Science, University of Nottingham (Malaysia Campus), Semenyih 43500, Selangor, Malaysia
[e] Material Processing Institute, Middlesbrough, TS6 6US, UK
[f] Department of Industrial and Systems Engineering, Khalifa University, Abu Dhabi, United Arab Emirates
[g] Departments of Materials Science & Engineering, The University of Sheffield, Sheffield, S1 3JD, UK
[h] Departments of Materials Engineering, NED University of Engineering and Technology, Karachi, Pakistan
[i] Materials Research Institute, The Pennsylvania State University, University Park, PA, 16802, USA

ARTICLE INFO

Keywords:
Energy harvesting
Thermoelectric module
Thermoelectric efficiency
Lifecycle Assessment
Power output

ABSTRACT

Due to high toxicity, thermal instability at high temperature, low availability, and the high cost of raw metallic alloys such as Bi_2Te_3 for thermoelectric (TE) applications, there has been a drive to develop earth-abundant and eco-benign TE materials suitable for high-temperature applications. Oxide-based TEs have lately been touted to satisfy these criteria, but a lifecycle assessment (LCA) and energy payback period (EPBP) assessment of both classes of materials have not been conducted. This paper presents a comparative LCA of two laboratory-based TE modules namely, non-oxide *n*-type selenium-doped Bi_2Te_3 and *p*-type antimony-doped Bi_2Te_3 (Module A) versus oxide-based *n*-type lanthanum-doped $SrTiO_3$ and *p*-type layered $Ca_3Co_4O_9$ (Module B). Electrical energy consumption (EEC) during fabrication constitutes the largest impact for both modules, even under a decarbonised grid scenario, although Module B has an overall lower EEC. Nonetheless, for Module A, the use of tellurium and antimony exhibited noticeable environmental toxicity impacts, but smaller compared to EEC. The rare earth elements contained in the *n*-type component of Module B, showed negligible environmental toxicity impact, but those from its *p*-type component is noticeably high due to the presence of cobalt oxide. Computations of performance characteristics based on the material configurations of both modules showed that Module A yielded a higher power output compared to Module B, and as the power output increases, the EPBP becomes almost identical for both modules, underscoring its integral role to EEC offsetting. Key challenges, therefore, once EEC is diminished for large-scale applications are raw materials availability and cost, alongside performance.

Introduction

Energy demand constitutes one of the most important and difficult challenges confronting humankind today, provoking social and political unrest worldwide. As such, the provision of adequate energy to meet the needs of a rapidly growing world population with rising standards of living will require a major transformation of the global energy systems. Achieving this whilst mitigating the risks of climate change is even more challenging. Thermoelectric (TE) materials, which convert heat into electrical energy and vice-versa could play a vital role towards attaining global sustainable energy solutions [1]. Home heating, factories, automotive exhaust, nuclear and thermal power plants, and other industrial processes all generate huge amounts of unused waste heat (Fig. 1), which could be transformed into clean electricity using TE devices/systems.

* Corresponding author at: WMG, The University of Warwick, Coventry, CV4 7AL, UK.
E-mail address: t.ibn-mohammed@warwick.ac.uk (T. Ibn-Mohammed).
[1] I.M. Reaney is the Principal Investigator on the grant.

https://doi.org/10.1016/j.ecmx.2023.100395
Received 21 March 2023; Received in revised form 11 May 2023; Accepted 22 May 2023
Available online 25 May 2023

Nomenclature

Abbreviations

AP	acidification potential
CC	climate change
CCO	p-type layered cobalt oxide
CED	cumulative energy demand
CML	Institute of Environmental Science, Leiden University
CO_2	carbon dioxide
CoAs2	smaltite
CoAsS	cobaltite
DALYs	disability-adjusted life years
EEC	electrical energy consumption
EoL	end of life
EP	eutrophication potential
EPBP	energy payback period
EQ	ecosystem quality
EU	European Union
FAETP 100a	freshwater aquatic ecotoxicity
FSETP 100a	freshwater sediment ecotoxicity potential
GHG	greenhouse gas
GWP	global warming potential
HH	human health
HTP 100a	human toxicity potential
IR	ionising radiation
kW	kilowatt
kWh	kilowatt-hour
LCA	life cycle assessment
LCI	life cycle inventory
LU	land use
MAETP 100a	marine aquatic ecotoxicity potential
ME	material embedded
MIPS	material input per service unit
MJ-eq	mega joule equivalent
MSETP 100a	marine sediment ecotoxicity potential
mW	milliwatt
NR	natural resources
POCP	photochemical ozone creation potential
REEs	rare earth elements
RIR	recycling input rate
RR	recycling rate
SbBT	p-type antimony-doped Bi_2Te_3
SDG	sustainable development goal
SeBT	n-type selenium-doped Bi_2Te_3
SLT	n-type lanthanum-doped $SrTiO_3$
SNT	n-type neodymium-doped $SrTiO_3$
SPS	spark plasma sintering
TAETP 100a	terrestrial ecotoxicity potential
TE	thermoelectric
TEG	thermoelectric generator
UPE	unit process exchange
W/m^2	watt per meter square
WEEE	waste electrical and electronic equipment

Symbols

E	electric field
E_p	embodied energy
P_{R_L}	power output delivered to the load resistance
Q_C	rate of heat input and heat removal at the cold junctions of the TEG
Q_H	rate of heat input and heat removal at the hot junctions of the TEG
Q_S	heat exchange
η_{TEG}	electrical efficiency
I	current
ρ	resistivity
m	number of couple
R_L	load resistance
β	Seebeck coefficient
T_C	cold junction temperature
T_H	hot junction temperature
V	voltage
V_s	open-circuit voltage difference
k	thermal conductivity
σ	electrical conductivity

TEs are solid-state devices that contain no moving parts, they are responsive, compact, silent, reliable, scalable, and feasible for miniaturization [2]. They require minimal maintenance, possess long lifetimes, and do not generate deleterious waste, rendering them ideal for small, dispersed power generation [1,3]. The Quadrennial Technology Review (QTR) by the US Department of Energy [4] reported that if TE generators with conversion efficiencies of 2.5% were integrated within chemical production, petroleum refining and iron and steel production, between 1,880 and 4,700 GWh/year waste heat could be recovered. Similarly, Funahashi and Urata [5] concluded that if 20% of waste heat from automobiles, power and incineration plants could be converted to electricity, 35,000 GW of power per year could be obtained, making TE generators viable options to increase the efficiency of energy production and usage [6]. Numerous authors have since demonstrated the energy-saving potentials of thermoelectric modules in different applications [7-12].

TE devices or generators (TEG) contain many thermocouples consisting of *n*-type (free electrons) and *p*-type (free holes) semiconducting materials (Fig. 2). The application of heat to one side of the module pushes electrons and holes from the hot side to the cold side, driving an electrical current to power an electric load through the external circuit [3]. The temperature difference provides the voltage ($V = \propto \Delta T$) based on the Seebeck effect. TE can also be operated in reverse as a heat pump to produce cooling based on Peltier effect ($Q = \propto TI$) where the external circuit is a d.c. power supply, which drives the electric current (I) and heat flow (Q) [1]. The maximum efficiency of a TE material for both power generation and cooling is determined by its figure of merit [1,3] $ZT = \left(\frac{S^2\sigma}{\lambda}\right)T$, a unitless combination of three properties that vary with temperature – electrical conductivity (σ, S/m), thermal conductivity (λ, W/mK) and Seebeck coefficient (S, μV/K).

A TE material should possess a high Seebeck coefficient, high electrical conductivity, and low thermal conductivity (λ, W/mK). A high electrical conductivity is essential to minimize Joule heating and low thermal conductivity assists in retaining heat, whilst maintaining a high-temperature gradient. ZT allows for the comparison of the efficiency of devices fabricated from different materials. $ZT = 1$ is considered good, but 3–4 is crucial to be competitive with regard to mechanical energy generation and refrigeration [1]. However, the best reported ZT values range between 2 and 3 because of the fundamental limit imposed by the nature of the three parameters – a large Seebeck coefficient requires low carrier concentration, yielding low electrical conductivity while low Seebeck coefficient materials provide a high electrical conductivity [14].

Currently, the most widely used TE materials are Bi_2Te_3 and Sb_2Te_3 due to their large ZT for both *n*- and *p*-type TE systems [1]. Due to high toxicity, thermal instability at high temperature, low availability, and high raw materials cost of metallic alloys such as Bi_2Te_3, there has been

a drive to develop earth-abundant, non-toxic, eco-benign and cheap TE materials suitable for high-temperature applications. Oxide-based TEs have shown potential concerning satisfying these criteria. However, a primary concern with this class of TE material is their relatively low ZT [2]. Despite this, it has been speculated that oxide-based TEs offer advantages in terms of environmental credentials and cost of raw materials over their non-oxide counterparts [2,13,14] Yet, a comparative environmental impact assessment of the lifecycle phases and energy payback period assessment of both oxide and non-oxide family of TE materials have not been conducted.

This paper, therefore, presents a comparative prospective lifecycle assessment (LCA) of two TE modules A and B at the laboratory level to assess their environmental impact. **Module A** is based on two representative *non-oxide* TE materials: ***n-type* selenium-doped Bi_2Te_3 (SeBT)** and ***p-type* antimony-doped Bi_2Te_3 (SbBT)** whereas **Module B** comprises two representative *oxide-based* TE materials: ***n-type* lanthanum-doped $SrTiO_3$ (SLT)** and ***p-type* layered cobalt oxide: $Ca_3Co_4O_9$ (CCO)**. Also considered for Module B is the ***n-type* neodymium-doped $SrTiO_3$ (SNT),** to ascertain which of lanthanum or neodymium constitutes a better dopant from an environmental sustainability perspective. There are numerous TE materials to consider but our focus on these two specific modules was informed by: i) the abundance of the constituent elements; ii) the extent to which they are studied (e.g. the most commonly studied non-oxide TEs are Se and Sb-doped Bi_2Te_3 [1] and the current leading contender for oxides are *p-type* layered cobalt oxide ($Ca_3Co_4O_9$) and rare-earth-doped $SrTiO_3$ [16–18]); iii) the level of their progress in terms of the gap between TE materials development and generators; iv) their potential impact on the TE materials market; and v) whether LCA has been conducted on the constituent materials in other applications (e.g. photovoltaics, piezoelectric etc.).

The focus on the representative candidate materials allows not only the valuation of the environmental profile of heavy-based metals, which are toxic and rare including Te and Bi (for non-oxides) and "eco-benign" and (comparatively) abundant elements such as Sr, Co, and Ti (for oxides) but also understanding of the environmental implications of the dopants, Sb/Se, and La_2O_3/ Nd_2O_3, used in Bi_2Te_3 and $SrTiO_3$, respectively. Furthermore, to understand the role of power output on how electrical energy consumption during fabrication is offset by TE energy production, a mathematical model that quantifies the electrical power output of a basic TE module has been developed. The mathematical model considers the rate of heat input from the waste heat source and heat removal at the hot and cold junctions of an isolated PN unit of a TEG device. To obtain expressions for the power output and energy payback, the model systematically: (i) connects the thermal diffusion, temperature gradient and current flow through the principle of conservation of energy; (ii) integrates the fundamental physical transport properties of TE materials in the form of thermal/electrical conductance and the Seebeck effect; and finally (iii) incorporates the effect of electrical efficiency and a load resistance across the TEG.

Considering the above, the remainder of the script is structured as follows. In section 2, an overview of the literature detailing the TE properties of various non-oxide vs. oxides TE materials, alongside their end-of-life, recovery, and recycling rates of the elemental material constituents, as well as a review of previous LCA of TE materials is presented. Section 3 describes the laboratory fabrication routes of the TE

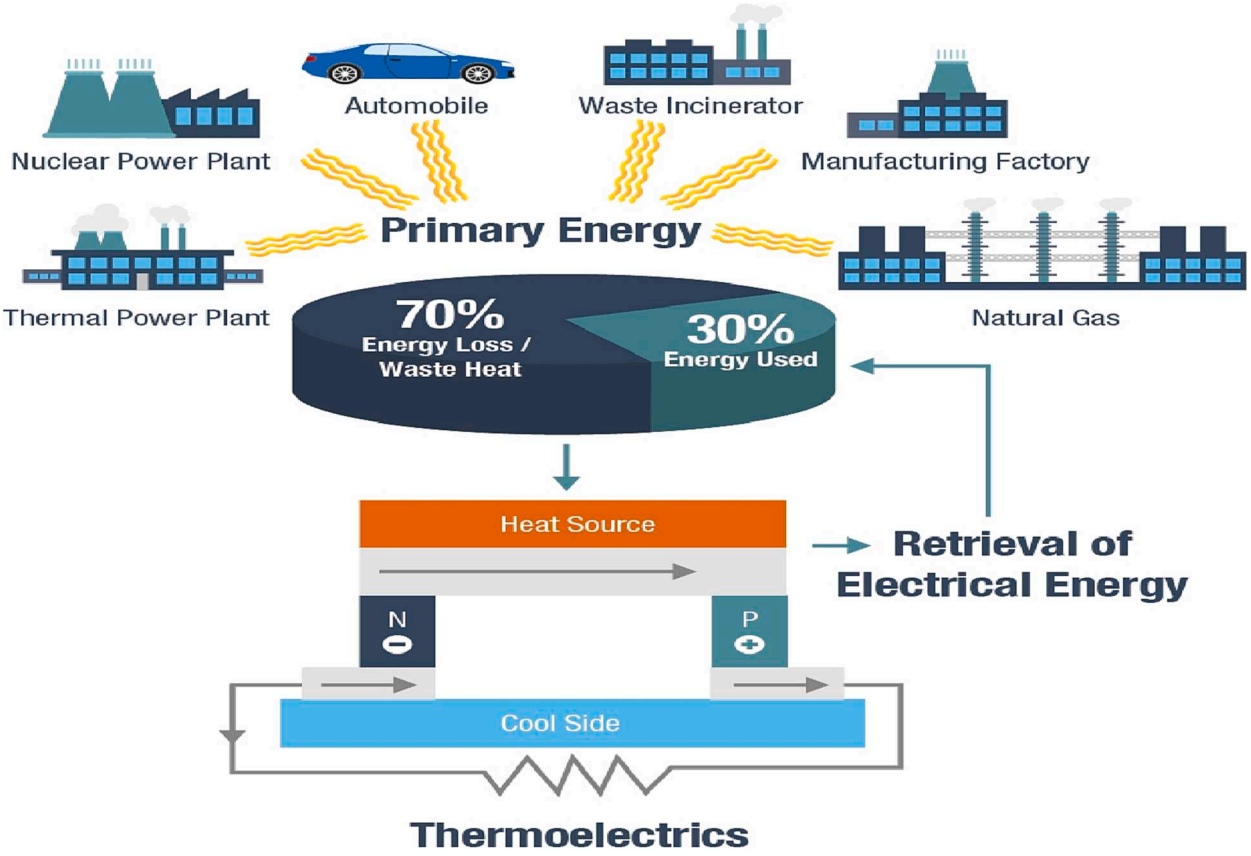

Fig. 1. Thermoelectric applications and system configuration. Illustration of how to improve the sustainability of the electrical energy base. Waste heat from factories, automobiles, nuclear and thermal power plants and similar sources constitute ~ 70% of all the energy generated by mankind[13]. This waste heat can be harnessed through the adoption of TE generators, for direct heat-electricity conversion, by leveraging their capability to process small, distributed power generation due to their high reliability, responsiveness, compactness, and noiseless and scalable characteristics. They can therefore play a significant role towards mitigating climate change whilst increasing energy efficiency[1]. TE can also operate reversely as a heat pump for refrigeration (cooling)[3].

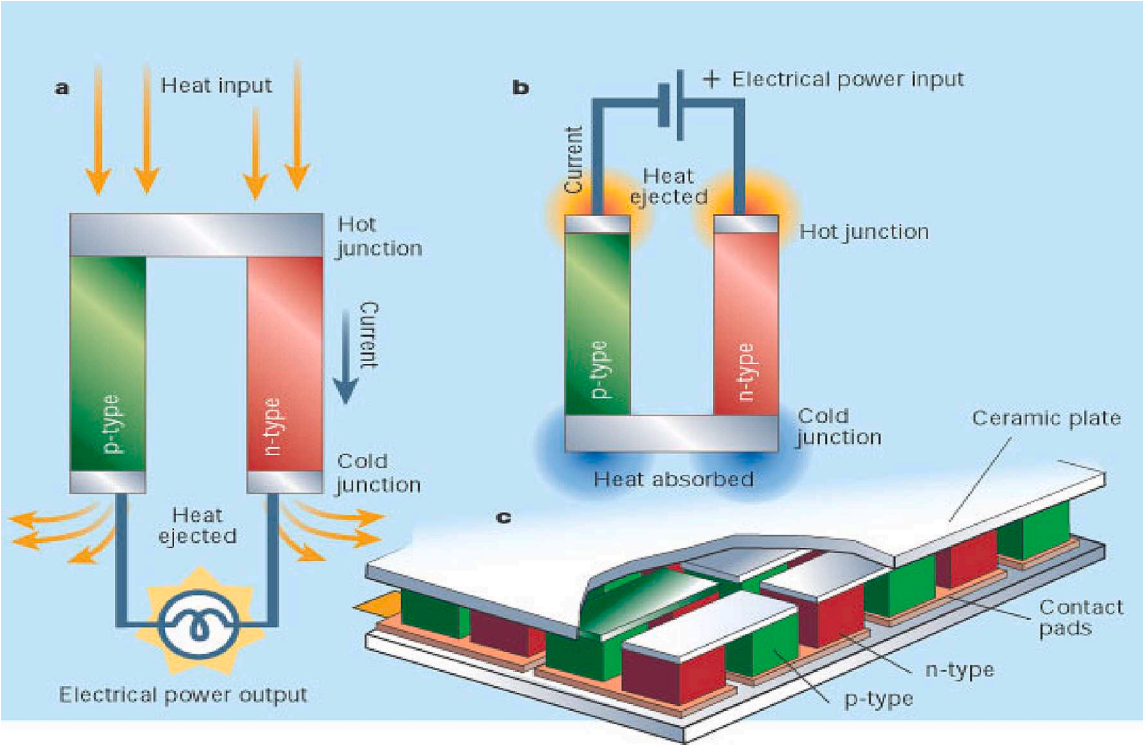

Fig. 2. Illustration of different modes of thermoelectric effect using a p-type (i.e., TE materials that possess positive Seebeck coefficients, containing free hole charge carriers) and n-type (TE materials that possess electron charge carriers and have negative Seebeck coefficients) materials. Small legs of n-type (red) and p-type (green) materials are connected electrically in series, thermally in parallel and then sandwiched between ceramic plates. For electrical generation, heat is applied to one side of the module, causing charge carriers to diffuse across the module and generating an electrical current: (a) mechanism of thermoelectric generation (Seebeck effect); (b) mechanism of thermoelectric cooling (Peltier effect) and (c) typical thermoelectric generator assemblage. Image source: ref [15]. (For interpretation of the references to colour in this figure legend, the reader is referred to the web version of this article.)

materials architectures analysed. Details of the general methodological notes for the LCA and the mathematical modelling framework for power output and energy payback period are presented in Section 4. In Section 5, the results, analysis, discussion, and limitations are presented, leading to conclusions in Section 6.

Literature review

This section elaborates on the key literature surrounding the investigations of TE characteristics of non-oxide vs. oxides TE materials, their end-of-life, recovery, and recycling rates of the elemental materials constituents, as well as an overview of previous LCA of TE materials.

Overview of performance characteristics of non-oxide vs. oxide-based TE materials

To date, leading TE materials are alloys such as Bi_2Te_3 [19], Sb_2Te_3 [1], PbTe [20-22], PbSe [23], SnTe [1] SnSe [24], $Mg_2Si_{1-x}Sn_x$ [25-27], clathrate [28,29], skutterudite [29,30], chalcogenides [29], half-Heusler alloys [29,31] and Zintl [32]. By far, the most widely used TE materials are Bi_2Te_3 and Sb_2Te_3 [1]. Bi_2Te_3 alloys possess the largest ZT for both *n*- and *p*-type TE systems for near-room temperature applications including refrigeration and waste heat recovery up to 473 K (Fig. 3a). PbTe, SnTe and $CoSb_3$ have been used for mid-temperature power generation (500–900 K) and silicon–germanium alloys have been successfully used for high-temperature (>900 K) TE generators [1] (Fig. 3a), although their ZT is fairly low. The majority of these TE materials suffer from several limitations including, chemical and thermal instabilities, low availability/high cost of raw materials and complex expensive processing [1,14]. Large-scale commercial applications are constrained by the presence of rare or heavy toxic elements (Fig. 3b) and the difficulty of conversion to engineering devices [14]. As such, high-performance TE materials based on non-toxic elements with high abundance in the earth's crust (Fig. 3b), and high chemical and thermal stability are pertinent for large-scale applications [33].

Oxide TE materials could play an important role towards the realisation of viable large-scale applications. Currently, their ZT is still relatively low and they are considered to be poor TEs due to low carrier mobility and high lattice thermal conductivity [2]. However, oxides possess numerous inherent advantages [34,35]. Their chemical and thermal stability allows for large temperature gradients thereby yielding high Carnot efficiency that compensates for low ZT [2]. Oxides are more stable at high temperature, Fig. 3a, and their chemical versatility and structural intricacy offer great flexibility for composition and structure [2]. The main challenge with oxides is their high thermal conductivity. Controlling the microstructure in $SrTiO_3$, for example, reduces the thermal conductivity due to increased grain boundary scattering [36]. Nano-structuring of oxides is a promising approach to reducing thermal conductivity without affecting electrical conductivity and the Seebeck coefficient. A number of novel concepts through which ZT in oxide TE materials can be enhanced is provided by He et al. [2]. Nevertheless, oxides of zinc, vanadium, tungsten, titanium, rhodium, molybdenum, manganese, copper, and cobalt exhibit a wide range of electronic properties pertinent to TEs. Layered cobaltite TEs such as Na_xCoO_2 and $Ca_3Co_4O_9$ exhibit the best *p*-type performance [13,36]. In contrast, *n*-type oxides with equivalent TE performance have yet to be discovered [14,37] with rare-earth-doped $SrTiO_3$ the current leading contender [16–18]. A summary of reported properties of several doped $SrTiO_3$ TE materials is provided by Lu et al. [16].

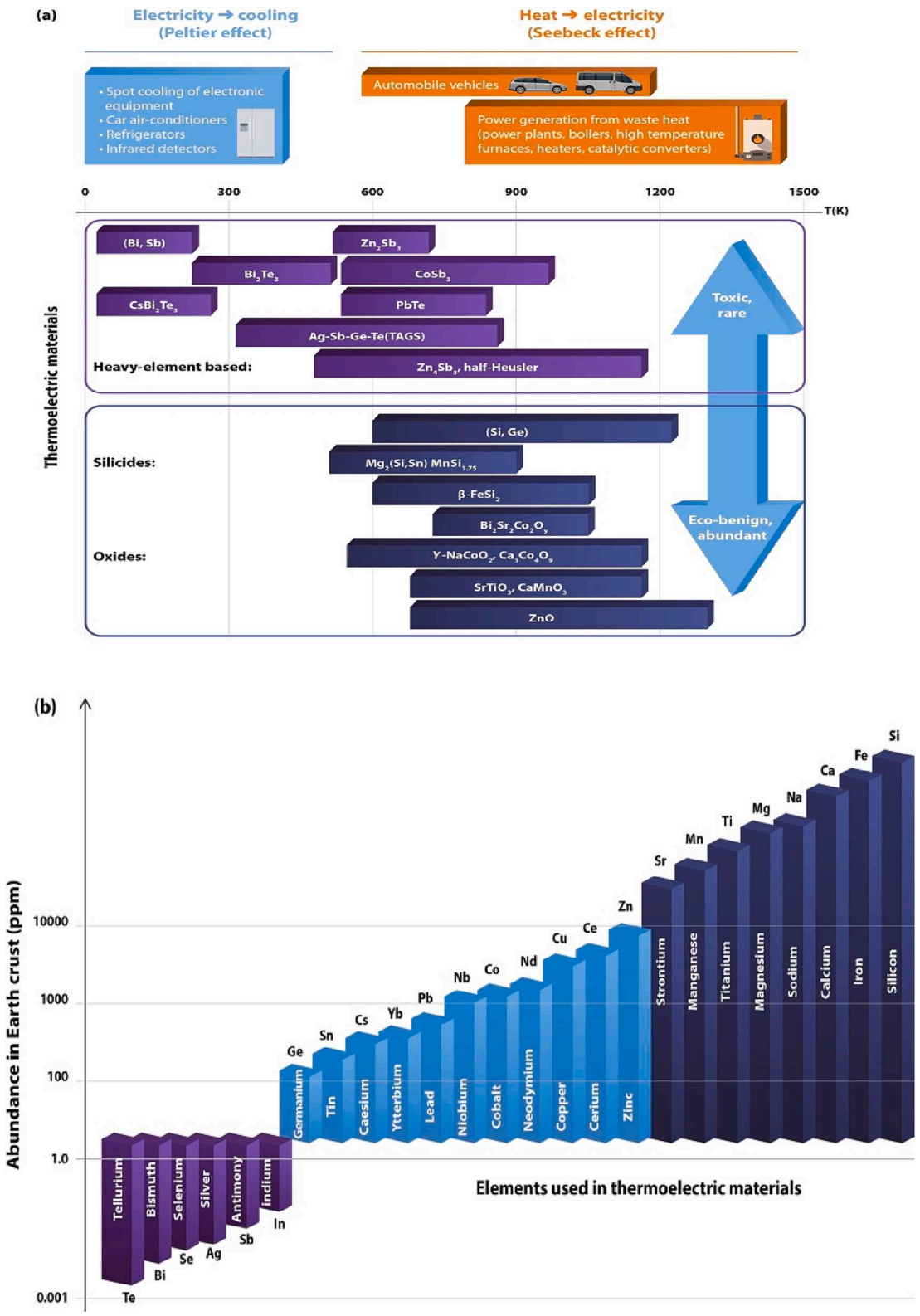

Fig. 3. Thermoelectric materials application and their abundance in the Earth's crust. (a) Schematic comparison of different TE materials for both power generation and cooling applications based on the temperature range of operation and the abundance in the Earth's crust of constituent elements. Bi_2Te_3 is by far one of the most widely used TE materials for near-room temperature applications including refrigeration and waste heat recovery. PbTe, SnTe and $CoSb_3$ have been used for mid-temperature power generation (500–900 K) and silicides such as (Si Ge) alloys have been successfully used for high-temperature (>900 K) TE generators. However, large-scale commercial applications have been constrained by the presence of rare or heavy toxic elements, prompting the need for high-performance TE materials based on non-toxic elements with high abundance. Oxides are particularly suitable for high-temperature power generation in the air; (b) Illustration of the abundance of elements used in TE materials. Elements represented by the purple bars are < 1 ppm; light blue bars are between 1.5 and 70 ppm; deep blue is > 100 ppm. The graph presented is not drawn to scale and is adapted with permission from ref [2]. (For interpretation of the references to colour in this figure legend, the reader is referred to the web version of this article.)

End of life, recovery, and recycling rates of elemental thermoelectric materials

At the end of life, TE materials join the millions of tonnes of waste electrical and electronic equipment (WEEE) generated annually at the global level. At a growth rate of 3–5% annually, WEEE is thought to be one of the fastest-growing global waste streams [38]. The Waste Hierarchy, outlined in the European waste directive 2008/98/EC, prioritises the prevention of waste ahead of reuse, recycling, other recovery techniques and disposal. Most metals are ideal candidates for the transition to a circular economy due to their inherent recyclability without the challenge of downcycling or quality loss. While the recycling rates of many metals are high (e.g. steel, aluminium, copper and lead), effort is needed to increase the recycling rates of other non-ferrous metals, precious and minor metals from end-of-life products such as electronics [39]. Recycling rates are hampered by product design, social behaviours, recycling technologies and the thermodynamic principles required for separation [40]. For those metals found in small amounts within a range of products, the increasing waste collection will yield increased recycling rates, though this is further hindered by global supply chains and poor recycling infrastructure [40].

Research into the end-of-life (EoL) management of WEEE has become prevalent in recent years, leading to the development of metal separation processes from the non-metallic components of WEEE. These processes include electrostatic and magnetic separation, hydrometallurgy, and bio-hydrometallurgy. It has been suggested that a hybrid approach, combining chemical and biological methods within a single process could lead to the most effective separation methodology [41]. From an environmental impact perspective, the hydrometallurgical and pyrometallurgical recycling processes allow metals to be recovered from WEEE, though pyrometallurgy results in waste gases and flue dust which contain halogens leading to potential human health issues and both hydro- and pyrometallurgy lead the production of an untreatable residue which must be landfilled [42,43].

Several TE materials contain rare earth elements (REEs) i.e., neodymium, cerium, and ytterbium, which have been classified as critical materials by different organisations [44-46]. Despite their high supply risk and the environmentally damaging nature of their extraction as virgin ores [44], their application continues to grow [47,48]. As supply risk decreases with increased recycling rates [44], improving the recycling technologies of REEs is key to reducing their criticality. While REE recycling is under development, it is also essential to ensure that the environmental impact of the recycling process is not more harmful to the environment than the benefits of material recovery [49]. This highlights the importance of the use of the LCA recycling methodology to compare the environmental impacts of products and processes before commercialisation [50].

Data regarding the recycling rate of materials relates to the efficiency of material reuse and can determine the effect of recycling on resource sustainability. This type of data is useful information for different stakeholders, such as governments to aid policy-making and industry for reporting purposes, and it can support further research into improving recycling technologies [51]. Monitoring and measuring recycling rates are reported in a number of different ways, examples include the EoL recycling input rate (RIR), Equation (1) [52] and the EoL recycling rate (RR), Equation (2) [51].

$$EoL_{RIR} = \frac{Inputofsecondarymaterial(fromoldscrap)}{Inputofprimarymaterial + Inputofsecondarymaterial} \quad (1)$$

$$EoL_{RR} = \frac{RecycledEoLmetal(oldscrap)}{EoLproducts(metalcontent)} \quad (2)$$

Fig. 4 provides the EoL-RIR (Equation (1) for some of the elements used in TE materials. The EoL-RR depends on the collection rate of the EoL products and the efficiency of the subsequent separation and preprocessing steps, all of which involve complex interactions of a wide array of players [53]. As previously highlighted, the recycling rates of TE metals such as copper and lead are high, whereas other non-ferrous metals, precious and minor metals suffer from low rates of recycling [39]. Lead is reported to have the highest recycling rate, at 75%, followed by silver at 55% [54]. While other sources, such as the United States Geological Survey, align with this data concerning lead recycling rates (given at 73%), this source reports the recycling rate of silver as 17% [55]. Furthermore, although the EU [54] report an EoL RIR value of 19% for titanium, Takeda and Okabe [56] submitted that this value may be as high as 90%. Sustainable Development Goal (SDG) number 12 (responsible consumption and production) incorporates indicator 12.5.1, which requires the reporting of national recycling rates in tonnes

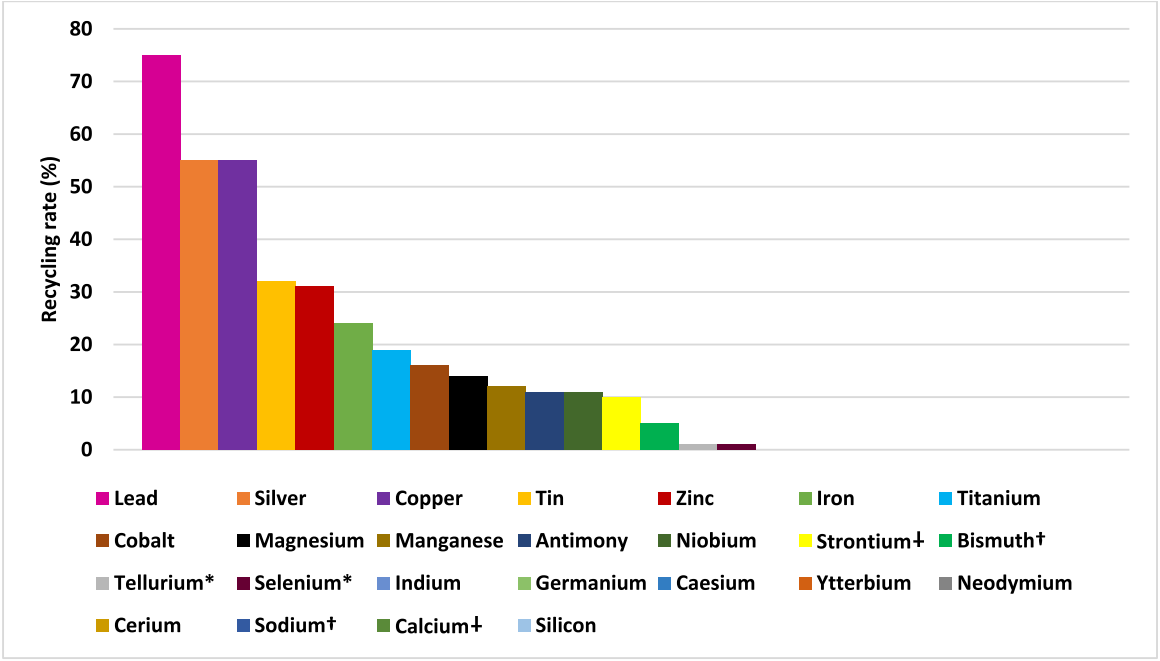

Fig. 4. End-of-life recycling input rates of the key elements used in thermoelectric materials. Sources: [54,58],†[55], ‡[59]. *End-of-life recycling rate.

of material recycled [57]. With the implementation of this indicator, a robust global average for the recycling rates of metals will be provided, further aiding governmental and industry decision-making practices. In Fig. 5, a periodic table representation of the global estimates of EoL recycling rates of sixty metals including elements used in thermoelectric is presented.

In the context of key metals used for TE applications as with other metals, their overall sustainability is predicated upon the collection rate of the EoL products that contain the materials and the efficiency of the subsequent separation and pre-processing steps involved in the recycling process [39]. The rate at which metals are successfully recycled obviates the requirements for their extraction from virgin ore. Despite the sustainability advantage and potential value, this presents, consumer and industrial products containing these materials have often been regarded as waste material as opposed to useful materials that can be put into other applications. Indeed, the mining and purification of rare-earth metals used in TE applications are not only expensive and labour-intensive, but it also takes a damaging toll on the planetary systems. Moreover, current approaches to recycling these materials are inefficient and wasteful. In an era where the planet's mineral deposits are becoming more prone to geological uncertainties and restricted ability to respond to increasing demand, there is a need to improve the recyclability of TE materials, which are found in numerous high-tech devices. Only then can their sustainability be rendered viable.

Review of previous LCA of thermoelectric materials

A considerable amount of literature exists on TE materials/performance characterisation, modelling of power outputs and waste heat recovery potential, and optimisation of energy conversion efficiency, among others. However, studies examining their lifecycle environmental impact are only just gradually gathering momentum. For instance, Soleimani et al. [60] conducted a comparative cradle-to-gate LCA of TE materials covering inorganic (e.g., Bi_2Te_3), organic (e.g., CNT/PEDOT:PSS) and hybrid (e.g., Te-PEDOT:PSS) types, based on five impact categories namely resource consumption, primary energy demand, waste, emissions and global warming potential. The authors concluded that inorganic TE materials constitute a significantly higher environmental impact compared to the other types considered, but noted that among the inorganic materials, Bi_2Te_3 was responsible for the lowest environmental impact. The huge environmental impact caused by inorganic materials stemmed from the extremely energy-intensive nature of the fabrication processes while the main concern for the organic and hybrid pertains to their low raw material supply requirements.

Patyk [61] carried out the comparative eco-efficiency lifecycle evaluations of TEGs with "steam expander" waste heat utilisation technology to ascertain the role of plant size on eco-efficiency and to identify the environmentally weak points of TEGs. The result indicates that under a wide range of conditions, the integration of TEGs for waste heat recovery offers reduced energy costs and environmental burden (i.e., they are more eco-efficient than "steam expander"). Even under less favourable conditions, energy savings and environmental benefits could be further achieved with additional expenditure. However, the author noted that under the upper power range the "steam expander" yielded improved and better performance in terms of eco-efficiency and electricity production. Patyk [62] also presented an overview of the environmental sustainability impact of TEGs used in various applications, covering resource availability, energy consumption during fabrication and potential energy/greenhouse gas (GHG) emissions savings, with a significant sectoral energy savings of $> 5\%$ in all applications considered. However, the focus was only on GHG emissions alone, neglecting other important environmental indicators.

Kishita et al. [63] (based upon their previous study Kishita et al. [64]), evaluated four life cycle scenarios of commercially-scaled TEGs based on Bi_2Te_3 installed in exhaust gas pipes of passenger automobiles in Suita City, Japan, based on technological performance and driving patterns, covering both environmental and economic aspects. By comparing the four scenarios, the authors reported that improvement of the TE figure-of-merit by a factor of 1.9 is required if the lifecycle CO_2 emissions are to be reduced to zero, based on the average driving pattern in the city. From an economic perspective, the authors noted that rendering TEGs profitable across their lifecycle would require approximately 10–40% reduction of their current price. However, a key limitation of this work was that it mainly focused on global warming potential, neglecting other important impact categories such as toxicity.

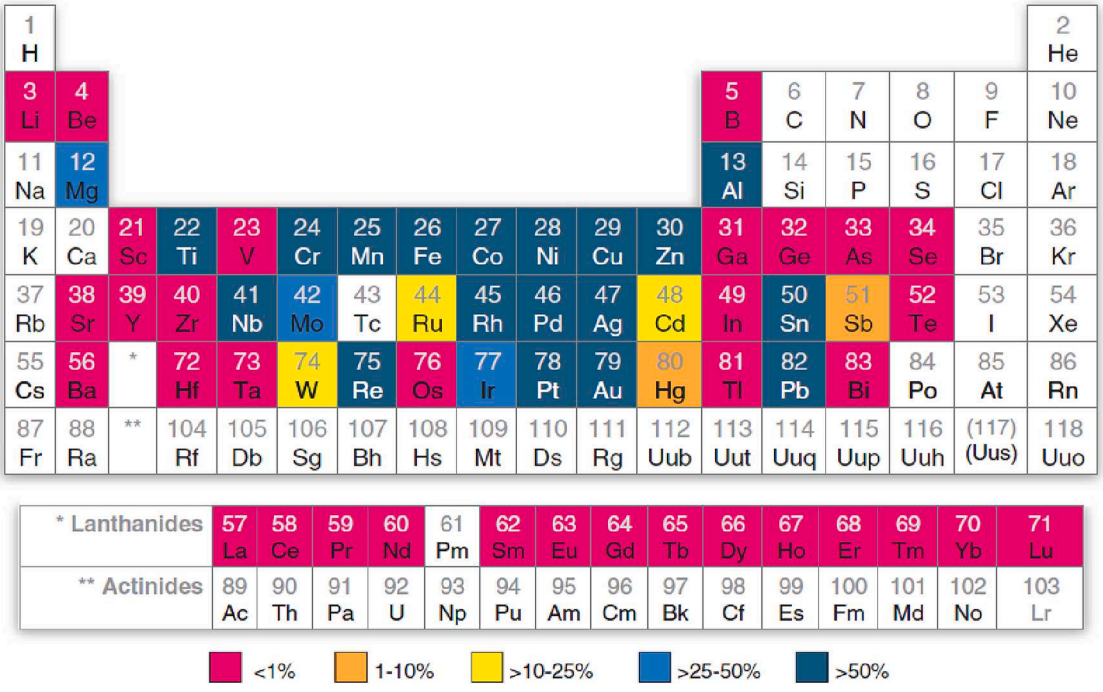

Fig. 5. Global estimates of EoL recycling rates of sixty metals including elements used in thermoelectric [40].

Iyer and Pilla [65] carried out the environmental profile evaluations of TE modules for applications with continuous waste heat generation via LCA based on five different TE materials configurations. This was based on numerous impact categories including toxicity, the scarcity of materials and end-of-life scenarios to demonstrate the ecological benefits and drawbacks of recycling TE materials. As with other authors, intense energy consumption during the fabrication of the module constitutes the major environmental hotspot, with material impacts showing negligible impact. The authors also noted that except under the application of a specific circular economy approach in specific instances to the TE materials, their end-of-life treatment has negligible effect on ecological impact.

Kawajiri et al. [66] conducted a cradle-to-grave LCA of TEGs in automobile applications, considering both environmental and social impacts. Two scenarios, namely the baseline scenario at 7.2% conversion efficiency and the technology innovation scenario (conversion efficiency of 17.7% at different production scale) was considered. Under the baseline scenario, GHG emissions across the lifecycle were positive but under the technology innovation scenario, the emission profile became negative due to the GHG credit accrued in the use phase. Based on the TEG configurations considered, the authors concluded that to reduce the overall impact attributed to TEG manufacturing and use, an increase in conversion efficiency of the TEG alongside a decrease in the number of materials (e.g., stainless steel) used in their construction is required. Irshad et al. [67] developed a procedure for evaluating the size, lifecycle CO_2 emissions and cost of building integrated TE air cooling and photovoltaic (PV) wall systems, in comparison with three categories of alternative cooling systems including grid and PV-connected systems. Their results indicated that the TE PV-connected system offered better economic, energy and carbon emissions saving potential compared to the other two systems, although the grid-connected system has a lower financial payback period due to the additional initial cost of the PV system. However, the authors ignored the impacts associated with the fabrication stage for both materials and device processing.

In their work, Sergienko et al. [68] employed LCA alongside material input per service unit (MIPS) analysis to scrutinise the environmental impacts of a single Bi_2Te_3 TE module and the associated impact of transporting the raw materials to the manufacturing site, based on photochemical ozone creation potential (POCP) and global warming potential (GWP). The electrical energy consumed during fabrication constitutes the main environmental hotspot under the two impact categories considered. However, other important aspects such as the impact of the elemental extraction and refining of the TE module were neglected, thus limiting the scope of the analysis. Søndergaard et al. [69] conducted an LCA of a new organic polymer TE material architecture based on roll-to-roll (R2R) technology which supports rapid processing of the materials. The overall embodied energy was evaluated to be 19.23 MJ with the polyethylene terephthalate (PET) substrate processing representing the biggest portion. Several other technical performance challenges were identified such as difficulty in thin-film TE development due to the influence of the substrate thickness on the thermal gradient of a device.

So far, there is little or no LCA work on oxide-based TE materials in comparison with non-oxide equivalents. Given the vital role that oxides could play in the realisation of viable large-scale TE applications, scrutinising their energy and environmental profile across different indicators to ascertain the merits or demerits of using them to replace non-oxide TE materials is key to advancing our understanding of their environmental implications. Besides, it will also facilitate informed decision-making for materials substitution strategies in TE applications.

Fabrication routes for Module a and Module B

A simplified fabrication procedure at the laboratory level temperatures and sintering times for the material architectures that constitute modules A and B are described in this section.

Fabrication route for TE non-oxide materials (Module A)

To date, bismuth telluride-based TE materials are the best-known materials having room temperature ZT values ~ 1. Bismuth telluride when suitably doped with either antimony or selenium yields TE properties leading to *p-type* and *n-type* behaviours, respectively [70]. In this work, two variants of Se and Sb-doped Bi_2Te_3 are considered namely *n*-type Bi_2Te_2Se and *p*-type $Bi_{0.5}Sb_{1.5}Te_3$. The synthesis routes were based on the work of Tang et al. [71] and Hu et al. [72,73] The *n-type* and *p-type* alloys (SeBT and SbBT) for Module A are melted for 10 h in an indirect arc furnace at 1073 K and 1023 K [71,73] at 50 V to 150 V [74] with several hundred amperes as secondary current. The power supply of the electric arc furnace is low-voltage and high-current due to [74]: *(i)* the high current required for obtaining high temperatures, since heating $Q \propto I^2$; *(ii)* the maximum secondary voltage, constrained to 275 V because of safety and insulation requirements; *(iii)* the large potential gradient between the electrodes because of the high voltage and charge which ionizes the nitrogen of the furnace atmosphere and *(iv)* the electrodes which are nearer to the charge so the arc remains away from the roof, increasing the life of the refractory.

Fabrication route for TE oxide materials (Module B)

The starting material constituents for the $Sr_{0.775}La_{0.15}TiO_3$ TE architecture are $SrCO_3$, TiO_2 and La_2O_3; and for $Sr_{0.775}Nd_{0.15}TiO_3$, the starting materials are the same except for the replacement of La_2O_3 with Nd_2O_3 with the view to ascertain which of them constitute a better dopant from an environmental sustainability perspective. Fig. 6 depicts the fabrication steps for both material systems. For the *p*-type layered cobalt oxide, synthesis via conventional solid-state reaction was achieved by using $CaCO_3$ and Co_3O_4 as starting precursors [75]. The precursors were thoroughly mixed in stoichiometric proportions in dry conditions, followed by ball milling for 48 h with an appropriate quantity of ethanol. The obtained dried mixtures were then calcined in air at 900 °C for 24 h to allow carbonate decompositions, thus forming the 349 phase. The resulting mixture was consolidated (i.e., reground and treated in vacuum (10^{-3} bar)) using Spark Plasma Sintering (SPS) technique, in which powder samples were loaded in a graphite die whose inner diameter is 20 mm. A pulsed electric current of 2500 A at a voltage of 4 V was passed through the assembly for heating towards the dwell temperature, maintained for 2 min under uniaxial pressure. The reference sample materials were achieved through the uniaxial cold pressing of the 349 powder at 92 MPa into pellets of appropriate thickness and diameter, followed by conventional sintering at 920 °C for 24 h with no pressure applied.

Methods

Life cycle assessment framework

This study adopts the LCA framework, which is based on four key steps [50]: (i) definition of goal and scope, where questions such as what, how and why pertaining to the LCA work are examined and where the systems boundaries and functional unit are established; (ii) analysis of the inventory in which inputs and outputs data for each process in the life cycle, as well as the emissions intensity of the associated impact categories, are systematically collected and integrated across the entire system; (iii) evaluation of the environmental effects, detailing the LCA calculations and results through classification and characterization for comparative analysis and (iv) the interpretation of the inventory and impact assessment of results, from where environmental hotspots are identified [76-78]. Process-based LCA formed the basis of the modelling.

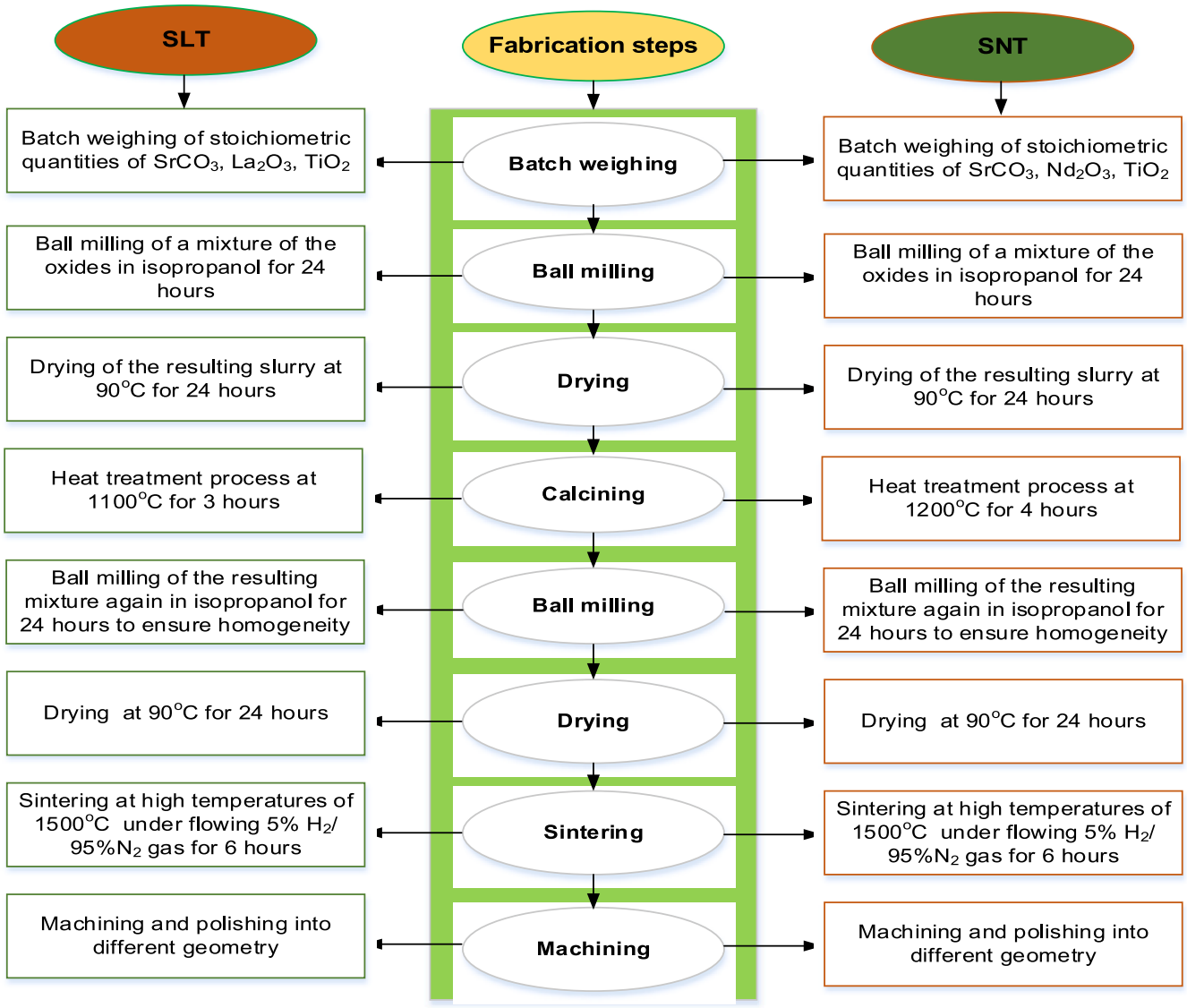

Fig. 6. Fabrication route of SLT and SNT thermoelectric materials. Ball milling entails the grinding of materials into very fine particles through a rotating or rolling jar. Calcination is a thermal treatment process in the absence or limited supply of air or oxygen applied to ores and other solid materials to bring about a thermal decomposition, phase transition, or removal of a volatile fraction. Sintering is a form of heat treatment to which powder compact is subject to impart strength and integrity. It entails compacting and forming a solid mass of material by heat and/or pressure without melting it to the point of liquefaction.

Goal, scope definition and functional unit for the LCA

The *goal* is to compare the environmental profile of laboratory-based non-oxide (Module A) and oxide-based (Module B) TE materials, based on a cradle-to-grave *system boundary*, Fig. 7. Module A is based on two representative *non-oxide* TE materials namely *n-type* selenium-doped Bi_2Te_3 (SeBT) and *p-type* antimony-doped Bi_2Te_3 (SbBT). Module B comprises two representative *oxide-based n*-type TE materials: *n-type* lanthanum-doped $SrTiO_3$ (SLT) and (ii) *p-type* layered cobalt oxide: $Ca_3Co_4O_9$ (CCO). The focus is at a laboratory level given the gap between TE materials development and generators, especially as it relates to the oxide-based counterparts.

For TEs, energy production depends on several factors, including TE efficiency, operating temperature, lifespan etc. As such, the *functional unit* could have been selected based on the conversion of exhaust heat to electricity at a specified TE efficiency over the lifespan of an automobile vehicle, for example. The total amount of electricity produced over the defined lifespan of the automobile can then serve as the reference flow that will be linked to the *functional unit* (e.g., the wattage of the system required to produce electricity). While such a *functional unit* is suitable for the well-established non-oxide TE considered due to their availability on a commercial scale and applications, it is not possible for the oxides-based TEs due to the reason highlighted above, thus rendering like-for-like comparison impossible.

Indeed, the analysed TE materials differ in the quantity of input energy they can harvest (per unit module) to produce electricity and it is a function of the temperature ranges (hot and cold junction temperatures) for optimal TE power output. We recognised that this hampers any immediate module comparison, but we are particularly interested in gaining an understanding of the role of the temperature difference and by extension the power output on the environmental profile and energy payback period of the TE materials analysed. The *functional unit* was therefore chosen based on the obligatory property that is required by the relevant market sector induced by environmental considerations, which in this case is the power output per unit area of the module (W/m^2), thus accounting for the energy production in the LCA conducted.

Lifecycle inventory and environmental indicators

Data requirements for the LCA of both modules are informed by

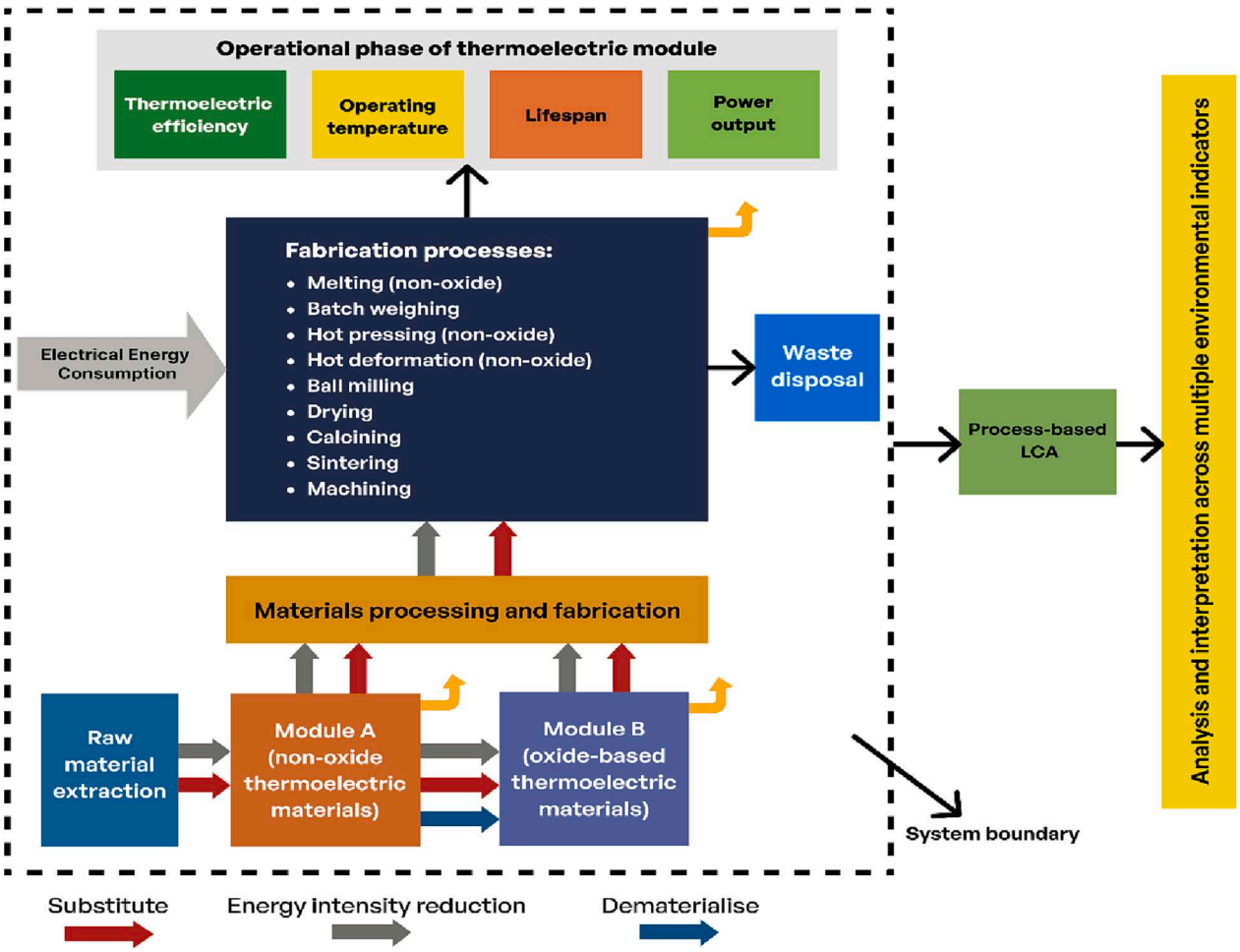

Fig. 7. System boundary defined for the LCA of two TE modules.

several steps including: (i) gaining an understanding of the non-oxide and oxide-based TE materials in terms of raw material requirements, costs, and synthesis/manufacturing routes; (ii) characterisation of the system boundary (Fig. 7) detailing materials and energy flows); (iii) construction of the lifecycle inventory (LCI) based on input requirements (i.e. physical processes), process, material and energy flows, and supply chain data. Process data for all identified material and process flows were based on inventory data estimated from laboratory processes (see Section 3) using engineering heuristics, stoichiometric relationships, the Ecoinvent database [79] and relevant data from within the literature. Electrical energy flow during fabrication was calculated by multiplying the electrical power specification of a given process equipment based on the manufacturer's description by the time in seconds, during which the specific temperature is maintained for each of the processes.

Emissions intensity data across all indicators considered for the materials and products including relevant environmental flows, such as raw material extraction, land use and emissions, as well as all material and energy inputs and products of activity were derived from the Ecoinvent database based on CML 2001 methodology [79]. For consistency and geographical representativeness, the data (the corresponding emissions intensities of the energy and materials) used in this study are based on the European market. In instances where data aren't available at the European level, data from other parts of the world are used as substitutes and the resulting outputs are largely valid on a global scale. For materials whose emissions intensity data were unavailable in the Ecoinvent database, they were derived based on stoichiometric reactions retrieved from previously published guidelines [80].

To provide a broad assessment of the environmental impact on the ecosystem, thirteen contrasting impact categories were selected for analysis and are expressed as "potential impacts". Thus, for example, GHGs are quantified as global warming potential (GWP, kg CO_2-eq); the acidification potential (AP, kg SO_2-eq) is a measure of the consequence of acids being emitted to the atmosphere and subsequently deposited in surface soils and watercourses. Eutrophication potential (EP, kg NOx-eq) is a measure of the pollution state of aquatic ecosystems in which the over-fertilisation of water and soil has turned into an increased growth of biomass. Materials utilisation (MU, MJ-eq) also known as the cumulative energy demand (CED) is a measure of the energy embodied in natural resources that have not undergone any anthropogenic conversion and need to be converted and transported to become usable energy (e.g., fossil fuels, solar energy, nuclear energy, geothermal energy, wind energy and biomass). CED of a product is therefore the addition of the aforementioned forms of primary energy. Land use (m^2a) is a measure of the environmental impacts related to physical occupation and transformation (i.e., reshaping and managing) of land areas for human purposes. Ionising radiation (DALYs) and malodours air (m^3 air) were also considered.

Five variants of ecotoxicity potential (kg 1, 4-DCB-eq): freshwater aquatic (FAETP 100a); freshwater sediment, (FSETP 100a); marine aquatic (MAETP 100a); marine sediment (MSETP 100a); and terrestrial (TAETP 100a), all of which are a measure of release of a toxic substance such as heavy metals into freshwater, marine water, and sediment environments, are considered. Human toxicity potential (HTP 100a) quantifies the potential human health problems caused by the release of toxic substances into the environment.

Separately, three endpoint indicators namely ecosystem quality (EQ), human health (HH) and natural resources (NR), following the Eco indicator 99 methodology [79] were also considered for the robustness of the analysis. EQ includes effects on species diversity especially as it relates to vascular plants and lower organisms based on four indicators namely ecotoxicity, acidification, eutrophication, and land use. NR entail the surplus or extra energy required in the future to extract minerals and fossil resources that are of lower quality. HH includes the number and duration of diseases and life years lost due to premature death resulting from environmental causes that stem from issues such as climate change and carcinogenic effects [81].

Impact assessment and interpretation

The next step is to adopt the inventory data developed to calculate the overall impact assessment of the modules across multiple environmental indicators using process-based LCA. Using LCIs, the process LCA can be expressed mathematically as:

$$ProcessLCA = \sum_{i=1}^{n} A_{p(i)} \times E_{p(i)} \tag{3}$$

where A_p is the inputs (i) into the product's supply chain including raw material extraction, energy consumption, material production and manufacturing processes, etc.; n is the total number of process input (i) into the product's supply chain, and E_p is the emissions intensity across multiple environmental indicators for each input (i) into a product's supply chain. Details of the life cycle inventory data that drives the process-based LCA can be found in the ESI. To establish the most impactful environmental indicators and their magnitude, the ten contrasting environmental impacts selected for the interpretation and analysis were normalised using Equation (4).

Normalised result of an impact category,

$$i = \frac{C_i}{n_i} \tag{4}$$

where C_i is the characterised result of impact category i and n_i is the normalisation reference of impact category i. The normalisation of the environmental impact results facilitates the comparison of all the variables, thus enabling a better understanding of the relative importance of the impact category results [82]. A global reference system [83] based on World 1995, was adopted to normalise the results. Due to the variability of non-renewable and renewable energy sources and the fact that their inclusion would not yield an accurate depiction of the distribution between each energy source, CED is excluded from the normalisation procedure. Malodour air was also excluded due to a lack of a normalisation reference factor. The final step in the LCA is the interpretation and analysis of the results, which is provided in Section 5. However, to account for the energy production by the TE modules, a mathematical model is presented in the next section.

Mathematical model of thermoelectric energy production

Several authors have attempted the development of mathematical models of TEGs for consideration in different applications [84-88]. From these studies, it has emerged that the energy conversion in TE generators depends on the fundamental physical transport properties of TE materials (thermal conductivity, electrical conductivity and the Seebeck effect). As a result, these properties appear prominently in the predictive model of functional characteristics of TE energy devices. As indicated in Section 1 and illustrated in Fig. 2, a TE power module consists of rows of integrated *p-type* semiconductor thermoelements possessing excess holes and *n-type* semiconductor thermoelements with excess electrons. Collectively, these thermoelements constitute the PN units that represent the active element of a TEG.

Here, the mathematical model of a basic TE module is presented. Following the practice in previous studies [84-88], the model of a TEG is developed by considering a single PN unit isolated from the TEG characterized by m number of PN couples. Along this vein, the following assumptions are considered: i) the TEG is ideally insulated from the surrounding heat transport phenomenon except at the junctions, where the thermal and electrical parasitic resistances are taken to be negligibly small; ii) the junctions of the unit are kept at T_H (hot junction) and T_C (cold junction), with $T_H > T_C$; iii) the thermal conductivity of the PN unit is constant; iv) the sign of the Seebeck coefficient of the *p*-type (β_p) and *n*-type conductors (β_n) in the unit are positive and negative, respectively, leading to an effective Seebeck coefficient for a PN unit as β_{pn}; v) the performance of the TE unit depends on the primary physical parameters of the TE elements (i.e., conductivity (σ), resistivity (ρ) and the Seebeck coefficient (β)).

Premised on the aforementioned perspective, the mathematical model of the TEG proceeds as follows. Let Q_H and Q_C be the rate of heat input (from the waste heat source) and heat removal at the hot and cold junctions of the TEG, respectively. Since a unit of the TEG is endowed with *p*-type and *n*-type legs through which heat conduction takes place in parallel, then Q_H and Q_C are split into two as: Q_{Hp} (p-type), Q_{Hn} (*p*-type); and Q_{Cp} (*p*-type), Q_{Cn} (*n*-type). The working mechanism of the TEG depends on the presence of a thermal load in the form of a temperature difference at the junctions, which then provokes thermal diffusion of the electrons and holes in the *p*-type and *n*-type legs. Consequently, the thermal diffusion generates an electrical output in the form of an open-circuit voltage difference (V_s) due to the Seebeck effect between the p-type and n-type legs as:

$$V_s = \beta_{pn}(T_H - T_C) \tag{5}$$

where $\beta_{pn} = (\beta_p - \beta_n)$ denotes the effective Seebeck coefficients of the semiconductors, which is related to the temperature gradient and the electric field E as [89]:

$$\beta_{pn} = \frac{E}{\Delta T} \tag{6}$$

The current flow in the conductor loop formed by the PN unit triggers the Peltier effect at both hot and cold junctions. The heat exchange (Q_S) at a junction J due to the Peltier effect is quantified as:

$$(Q_S)_J = \beta_{pn} T_J I \tag{7}$$

where T_J equals T_H or T_C at either the hot or cold side, respectively. Since thermal conduction also occurs due to the heat input at the hot junction, one may superimpose the Seebeck/Peltier and the thermal conduction effects and the principle of conservation of energy can be invoked for thermoelectric elements. On the cold side ($x = 0$), this reads:

$$Q_{Cp} = \beta_p(T_C I) - \sigma_p A_p \left.\frac{dT}{dx}\right|_{x=0} \tag{8a}$$

$$Q_{Cn} = -\beta_n(T_C I) - \sigma_n A_n \left.\frac{dT}{dx}\right|_{x=0} \tag{8b}$$

Similarly, on the hot side ($x = L$), the conservation of energy takes the form:

$$Q_{Hp} = \beta_p(T_H I) - \sigma_p A_p \left.\frac{dT}{dx}\right|_{x=L} \tag{9a}$$

$$Q_{Hn} = -\beta_n(T_H I) - \sigma_n A_n \left.\frac{dT}{dx}\right|_{x=L} \tag{9b}$$

where A and L denote the cross-sectional area and the geometric length of the thermoelectric elements. In Eqns. (8) – (9), Fourier's law relating the proportionality of thermal conduction with the ensuing temperature gradient has been employed. According to [90], the temperature gradient can be related to joule heat per unit length of the thermoelectric

elements as:

$$-\sigma_p A_p \frac{d^2T}{dx^2} = \frac{\rho_p I^2}{A_p}; \text{or} -\sigma_n A_n \frac{d^2T}{dx^2} = \rho_n I^2/A_n \quad (10a,b)$$

Integrating Eq. (10) produces the following relationships:

$$T(x) = \frac{1}{\sigma_p A_p}\left[\frac{\rho_p I^2}{A_p}x^2 + C_1 x + C_2\right] \text{or} T(x) = \frac{1}{\sigma_n A_n}\left[\frac{\rho_n I^2}{A_n}x^2 + C_1 x + C_2\right] \quad (11a,b)$$

where C_1 and C_2 are constants of integrations. The constants are determined by applying the boundary conditions that: (a) at $x = 0$, $T(x) = T_C$; and (b) at $x = L$, $T(x) = T_H$. The application of the boundary conditions leads to:

$$T(x) = \frac{1}{\sigma_p A_p}\left[\frac{\rho I^2}{A_p}x^2 + \left(\frac{(T_H - T_C)}{L} - \frac{\rho_p I^2 L}{A_p^2 \sigma_p}\right)x + T_C\right] \text{Or}$$

$$T(x) = \frac{1}{\sigma_n A_n}\left[\frac{\rho I^2}{A_n}x^2 + \left(\frac{(T_H - T_C)}{L} - \frac{\rho_n I^2 L}{A_n^2 \sigma_n}\right)x + T_C\right] \quad (12a,b)$$

Based on Eqns. (12), it is possible to obtain the temperature gradient term appearing in Eq. (9) as:

$$\sigma_p A_p \frac{dT}{dx} = -\frac{\rho_p I^2\left(\frac{L}{2} - x\right)}{A_p} + \frac{(T_H - T_C)\sigma_p A_p}{L} \quad (13a)$$

$$\sigma_n A_n \frac{dT}{dx} = -\frac{\rho_n I^2\left(\frac{L}{2} - x\right)}{A_n} + \frac{(T_H - T_C)\sigma_n A_n}{L} \quad (13b)$$

With Eqn. (13), the energy equations simplify, at the cold side ($x = 0$), to:

$$Q_C = (\beta_p - \beta_n)T_C I + \left(\frac{\sigma_p A_p}{L} + \frac{\sigma_n A_n}{L}\right)(T_H - T_C) - \left(\frac{\rho_p L}{A_p} + \frac{\rho_n L}{A_n}\right)(I^2/2) \quad (14)$$

Similarly, on the hot side ($x = L$), the conservation of energy takes the form:

$$Q_H = (\beta_p - \beta_n)T_H I + \left(\frac{\sigma_p A_p}{L} + \frac{\sigma_n A_n}{L}\right)(T_H - T_C) - \left(\frac{\rho_p L}{A_p} + \frac{\rho_n L}{A_n}\right)(I^2/2) \quad (15)$$

where K (internal thermal conductance of a PN couple) and R(internal electrical resistance of a PN couple) are retrieved from either Eqn. (14) or (15) as [88]:

$$K = \left(\frac{\sigma_p A_p}{L} + \frac{\sigma_n A_n}{L}\right); \text{and} R = \left(\frac{\rho_p L}{A_p} + \frac{\rho_p L}{A_p}\right) \quad (16)$$

Subtracting Eqn. (14) from (15), bearing in mind Eqn. (16), one may obtain the electric output power of the PN unit within the thermoelectric generator as:

$$P_{unit} = (\beta_p - \beta_n)_H I T_H - (\beta_p - \beta_n)_C I T_C - I^2 R \quad (17)$$

If there are m number of PN couples, then the total power output of the TEG is computed as:

$$P = m\left((\beta_p - \beta_n)_H I T_H + (\beta_p - \beta_n)_C I T_C - I^2 R\right) \quad (18)$$

However, it is noted that Eqn. (18) is based on the internal resistance of the PN couple (R). Typically, the working of the TEG demands that an external load resistance (R_L) is connected across the TEG device. When this happens, then the current I is determined as:

$$I = \frac{mV_s}{m\left(\frac{\rho_p L}{A_p} + \frac{\rho_p L}{A_p}\right) + R_L} = \frac{mV_s}{mR + R_L} = \frac{m\left((\beta_p - \beta_n)_H T_H - (\beta_p - \beta_n)_C T_C\right)}{mR + R_L} \quad (19)$$

Thus, the power output delivered to the load resistance becomes:

$$P_{R_L} = I^2 R_L = \left(\frac{m\left((\beta_p - \beta_n)_H T_H - (\beta_p - \beta_n)_C T_C\right)}{mR + R_L}\right)^2 R_L \quad (20)$$

In reality, the maximum current can only be delivered when the total internal resistance (mR) equals the external resistance load [91]. That is:

$$P_{\max} = I^2 R_L = \left(\frac{m\left((\beta_p - \beta_n)_H T_H - (\beta_p - \beta_n)_C T_C\right)}{2R_L}\right)^2 R_L = \left(\frac{m\left((\beta_p - \beta_n)_H T_H - (\beta_p - \beta_n)_C T_C\right)}{2}\right)^2 \frac{1}{R_L} \quad (21)$$

The electrical efficiency (η_{unit}) of a specific PN couple is found by taking the ratio of the power output and the rate of heat supply (Q_H) is established as [87]:

$$\eta_{unit} = P_{unit}/Q_H \quad (22)$$

However, as noted in previous studies [84,88,91], the overall electrical efficiency (η_{TEG}) of the TEG device is established by taking the ratio of the power output yielded to the external load and the rate of heat supply as:

$$\eta_{TEG} = P_{max}/(mQ_H) \quad (23)$$

Eqn. (24) facilitates a comparison of the performance of different types of materials for the design of efficient TEG devices. The energy payback time is calculated for r number of days in a specific number of years as:

$$E_{pb} = E_p / \int_0^r P_{max} dt \quad (24)$$

where E_p is the embodied energy used in producing the module.

In Section 5, the detailed interpretations of the modelling outputs are presented.

Results, analysis, and discussion

As stated in section 4.1.2, thirteen impact categories based on the CML 2001 methodology were considered from the onset. However, presenting and analysing numerous impact categories without considering which of them have an appreciable impact could potentially lead to a misplacement of priorities in terms of which impacts are truly important or whether attention should be focused elsewhere, thus allowing resources and intervention options to be more effectively directed. By using Equation (4) based on the characterised results of all the thirteen impact categories and their corresponding global normalisation reference data (see ESI), the most dominating impacts are shown in Fig. 8. As indicated, impact categories including climate change (CC), acidification potential (AP), eutrophication potential (EP), land use (LU), human toxicity (HT) and terrestrial ecotoxicity (TE) are negligibly small and therefore insignificant in the assessment of TE materials as they constitute < 2% of the impact. In the analysis and discussion that follows, attention is therefore focused on freshwater aquatic (FAE); freshwater sediment (FSE); marine aquatic (MAE); marine sediment (MSE) ecotoxicities alongside ionising radiation (IR). Material utilisation (MU), which is not among the normalised impact categories is also separately considered due to its importance in providing a measure of the energy embodied in the raw materials for TE applications.

Lifecycle impacts of fabrication of Module A

Fig. 9a(i) establishes that the electrical energy consumption (EEC) during the fabrication of *n-type* SeBT constitutes the largest

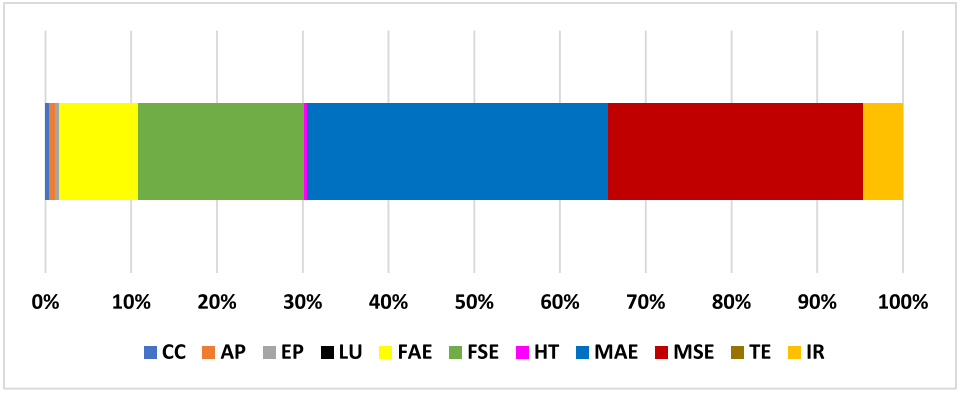

Fig. 8. Normalised results showing the most dominating impact categories.

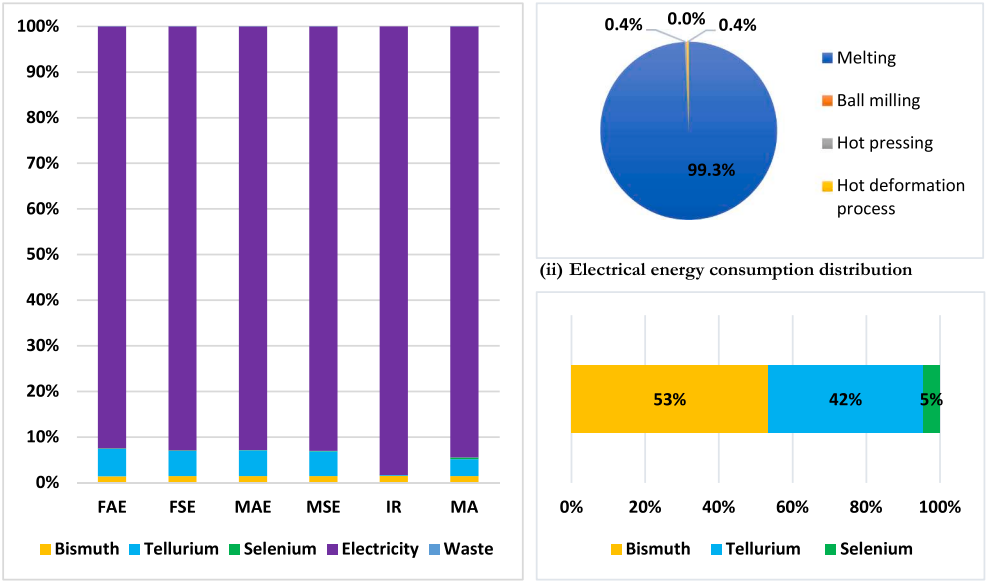

(i) Environmental profile

(ii) Electrical energy consumption distribution

(iii) Material utilisation distribution

Fig. 9a. Process group environmental impact of Module A. (i) Environmental profile of W/m^2 functional unit of laboratory-based ***n-type* SeBT** TE materials, showing relative proportions of each of the impact categories. Each coloured section represents the environmental impact of the unit process exchange. Energy and material inputs data are assessed based on seven environmental indicators, normalised to ensure the indicator of each category is 100%. **(ii)** distribution of EEC during fabrication. **(iii)** material utilisation impact distribution.

environmental impact across all indicators under consideration. For instance, EEC is the largest contributor to FAETP (92%), FSETP (93%), MAETP (93%), MSETP (93%), MA (94%) and IR (98%). The use of tellurium contributes 6%, 6%, 6%, 5% and 4% respectively to the aforementioned impact categories with negligible IR impact. Other materials have negligibly small impacts. Enormous electrical energy is required during SeBT fabrication due to the large power requirement of melting the elemental metal mixtures across the long duration and high temperature, representing 99% of the EEC. The remaining 1% is attributed to ball milling, hot pressing, and hot deformation processes, Fig. 9a (ii). Disaggregation of embodied material impact in SeBT manufacturing (Fig. 9a(iii)) shows that bismuth resulted in the highest material impact, contributing 53%. Tellurium and selenium are responsible for 42% and 5%, respectively.

When Bi_2Te_3 is doped with antimony as against selenium to fabricate the *p-type* SbBT, EEC during fabrication also constitutes the largest impact across all indicators, with some degree of impact from tellurium and antimony (Fig. 9b(i)). For instance, tellurium also constitutes a slight environmental impact across some indicators: 8% each for FAETP and MAETP; 7% each for FSETP and MSETP; and 7% for MA and zero IR impact. The presence of antimony also contributes 20% FAETP; 19% FSETP, 18% MAETP, 17% MSETP and 7% MA. EEC due to melting was also responsible for 99% of the impact, similar to SeBT, Fig. 9b(ii). In terms of the material impact of SbBT, tellurium constitutes the highest (64%), with antimony and bismuth representing 22% and 14% respectively (Fig. 9b(iii)).

Tellurium is regarded as the rarest stable solid element in the Earth's crust and is eight times less abundant than gold [92]. It is mined only in minute quantities and recovery poses serious technological and economic challenges [93]. Roughly 90% of tellurium is produced from copper anode slimes from electrolytic refining of blister copper and its recovery and recycling are energy intensive [94]. Small quantities of tellurium are less toxic than selenium due to easier reduction to metal [95]. Its toxicity depends on its oxidation state, e.g. Te^{4+} is ten times more toxic than Te^{6+} but is not carcinogenic [96]. The overall health hazard of tellurium is determined through the route and duration of exposure. Short-term exposure causes dizziness, loss of appetite, nausea, dermatitis and headaches and it produces a metallic taste and dryness in the mouth [97]. Long-term exposure leads to the build-up of fluids in the lungs and the destruction of red blood cells [98].

Man-made release of antimony can occur in water and air through waste incinerators, mines and industrial facilities and is toxic to aquatic life [99]. The level of harm to humans is a function of the dose, duration, frequency, and route of exposure (e.g., breathing, drinking, eating or skin contact). Chronic exposure to antimony at levels of 9 mg/m^3 in the air may result in irritation of the eyes, lungs and skin [100]. Inhalation

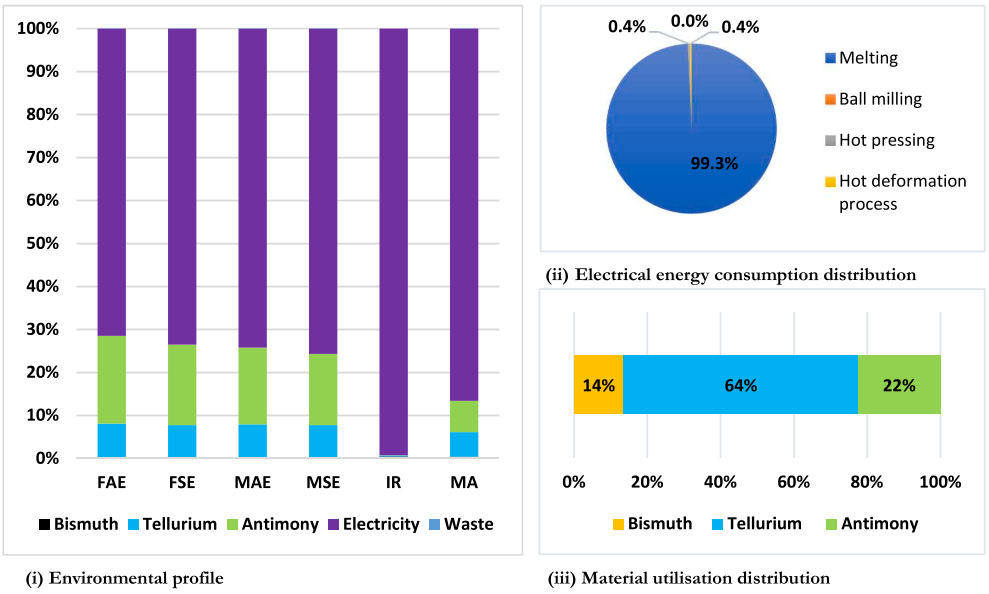

(i) Environmental profile

(ii) Electrical energy consumption distribution

(iii) Material utilisation distribution

Fig. 9b. Process group environmental impact of Module A. (i) Environmental profile of W/m^2 functional unit of laboratory-based ***p-type* SbBT** TE materials, showing relative proportions of each of the impact categories. **(ii)** distribution of electrical energy consumption during fabrication. **(iii)** material utilisation impact distribution.

of antimony over the long-term leads to stomach pains and ulcers, pneumoconiosis, diarrhoea and vomiting [100]. Although antimony is extremely useful, measures must be put in place to avoid exposure. Roughly 90–95% of bismuth is derived as a by-product of lead and copper smelting with high energy required for purification and refining, posing extra challenges in recovery [101]. The recycling of bismuth is difficult due to the high energy consumed, rendering it a material for one-shot applications [101]. Consequently, bismuth possesses a recycle fraction of between 9 and 10% [102]. In the next section, the discussion and analysis of the environmental impact of oxide-based TE materials (Module B) are provided.

Lifecycle impacts of fabrication of Module B

As with non-oxide TE materials, EEC during the fabrication of oxides also constitutes the largest environmental impact across all indicators considered. For instance, the *n-type* SLT (Fig. 10a(i)), EEC is responsible for 98% of all impact categories except under MA where it is responsible for 88%. The impact of other input materials (i.e., strontium carbonate and lanthanum oxide) into the unit process exchange of SLT is negligibly small. At the laboratory level, the effect of substituting lanthanum oxide with neodymium oxide in the *n-type* TE material architecture was carried and EEC also constitute the highest impact for SNT in a similar fashion to SLT with a negligibly small impact of neodymium oxide (see ESI for details). A detailed breakdown of EEC and material utilisation

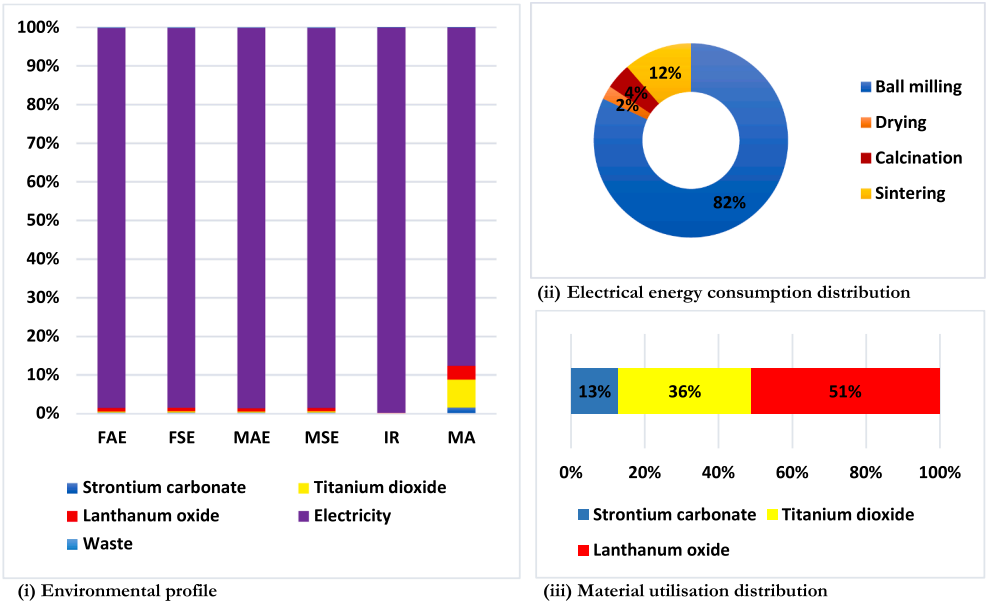

(i) Environmental profile

(ii) Electrical energy consumption distribution

(iii) Material utilisation distribution

Fig. 10a. Process group environmental impact of Module B. (i) Environmental profile of W/m^2 functional unit of laboratory-based ***n-type* SLT** TE material, showing relative proportions of each of the impact categories. **(ii)** distribution of electrical energy consumption during fabrication. **(iii)** material utilisation impact distribution.

from contributing processes and materials for the fabrication of SLT is provided in Fig. 10a(ii) to 10(iii) respectively. For SLT, ball milling, sintering, calcination, and drying are responsible for 82%, 12%, 4% and 2% of EEC respectively. In terms of material impact, lanthanum oxide contributes 51%, titanium oxide (36%) and strontium carbonate (13%). Although both SLT and SNT were environmentally scrutinised, however, SLT is preferred to SNT due to the very high cost of Nd_2O_3 compared to La_2O_3, which may constitute a major hindrance to its wider adoption when transitioning from laboratory to market. Attention is therefore focused on SLT as the *n-type* leg of Module B in the remainder of the comparative analysis.

Both SLT and SNT contain rare earth elements (REEs) whose criticality has been highlighted by the European Union Commission [103] but with negligible environmental impact across all indicators examined in this work. With such an insignificant impact, they are unlikely to pose any threat regarding their application in the development of oxide-based TEs. Although these materials are not rare, difficulties in their mining in unfeasibly economic concentrations, monopolistic supply conditions and high demand constitute a problem [104,105]. Their production routes cause a number of environmental issues including wastes from mining, GHG emissions/pollution, hazardous wastewater discharge and resource depletion [106,107]. Currently, the methods of separating REEs for recycling are not only energy-consuming, labour-intensive, and expensive, but they also require massive amounts of solvents. Simpler methods for targeted separations of mixtures of REE salts are currently being developed [108].

Fig. 10b shows the environmental impact of the *p-type* layered cobalt oxide TE material. As shown, EEC during fabrication also constitutes the highest impact: FAETP (72%), FSETP (90%), MAETP (74%), MSETP (70%), MA (47%) and IR (97%). However, the presence of cobalt oxide poses a considerably high environmental impact, contributing 28%, 30%, 26%, 28% 52% and 3% respectively to the aforementioned impact categories, Fig. 10b(i). EEC breakdown (Fig. 10b(ii)) shows ball milling consuming the largest energy portion (64%). Based on material impact disaggregation, the use of cobalt oxide dominates at 98%.

Cobalt is a precious metal which is commonly distributed naturally in soils, rocks, water, and vegetation and always occurs in the earth's crust in association with nickel alongside arsenic in some instances [109], and once it enters the environment, it cannot be destroyed [110]. It is used in numerous industrial and military applications [111]. Smaltite (CoAs2) and cobaltite (CoAsS) constitute important cobalt minerals, but their main sources are speisses, which are derived as a co-product of arsenic ores of copper, nickel, and lead production [109]. Depending on the ore grade, surface type and size, the extraction routes of cobalt could be through underground or open-cast methods or a hybrid of both [112]. The ore is further processed in beneficiation to produce a concentrate alongside other processes (e.g., calcining, smelting etc) for metal selection and further concentration [79].

All the above processes involved in the extraction of cobalt and by extension its oxides have a high cost to the environment due to the release of harmful wastes that affects groundwater and ecological land resources and air quality. For instance, during the mining and extraction of cobalt, the particles emitted consist of radioactive emissions and other dangerous particles which may cause cancer, vomiting and nausea, vision, and heart problems as well as thyroid damage [113]. Exposure to high concentration of cobalt may also result in pneumonia or asthma and contaminated soils due to accumulated cobalt particles may also affect the natural ecosystems [113]. A range of mechanisms for reducing the impact of cobalt is provided by Farjana et al. [113].

Lifecycle impacts comparison based on eco indicator 99 methodology

For robustness of the analysis, all the unit process exchanges for Modules A and B are analysed based on three endpoint indicators (Fig. 11 (a-d)): ecosystem quality (EQ), human health (HH) and natural resources (NR). As with the CML 2001 method, energy consumption during fabrication dominates across all the endpoint indicators, with materials like cobalt oxide, antimony, and tellurium also showing relatively high impacts. The reasons for this environmental profile are as already captured in Sections 5.1 and 5.2.

Environmental profiles comparison of modules a and B

Fig. 12 shows the comparison of the environmental profile of Module A vs. Module B. Module A generates a significantly higher environmental impact across the categories considered. The fabrication of SeBT and SbBT TE materials in Module A consumed enormous electrical energy (~339 kWh for both) due to the large power requirement of melting

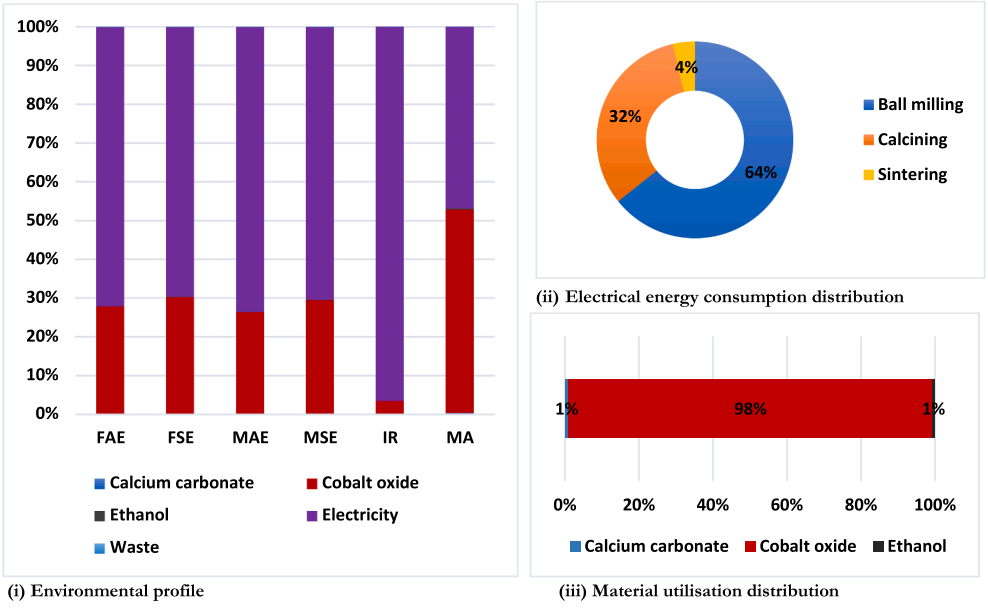

(i) Environmental profile

(ii) Electrical energy consumption distribution

(iii) Material utilisation distribution

Fig. 10b. Process group environmental impact of Module B. (i) Environmental profile of W/m^2 functional unit of laboratory-based **layered cobalt oxide (*CCO*)** TE material, showing relative proportions of each of the impact categories. **(ii)** distribution of electrical energy consumption during fabrication. **(iii)** distribution of material utilisation impact.

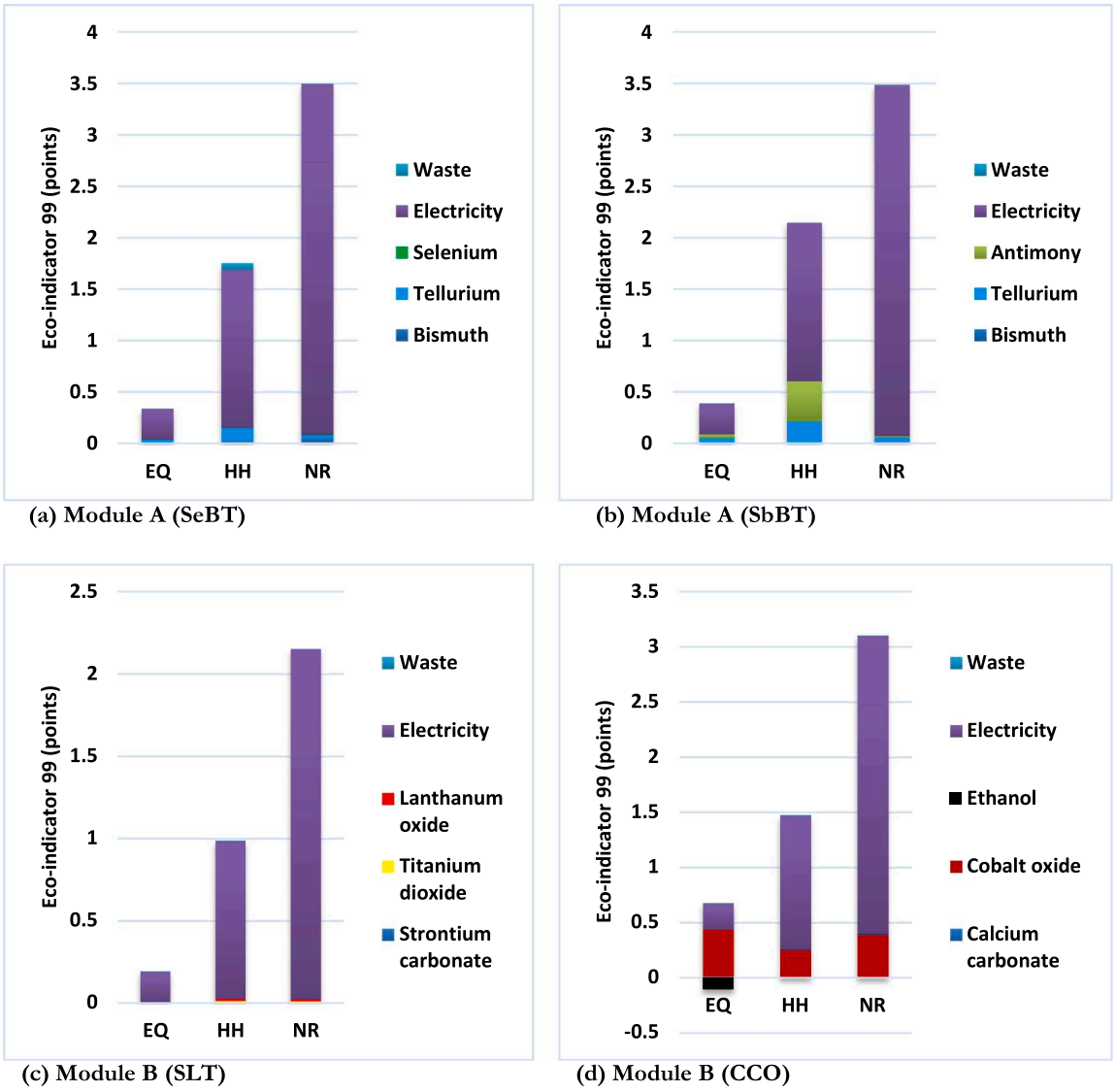

Fig. 11. Life cycle impacts comparison based on Eco-indicator 99 methodology.

the elemental metal mixtures across the long duration and high temperature, Fig. 12a. The antimonide content in the SbBT yielded a significantly higher specific heat compared to SeBT. Module B consumed a total of ~ 240 kWh for both materials, however, the SLT component consumed less (105 kWh) due to a shorter duration for calcination (4 h at 1200 °C) compared to CCO which was calcined in air at 900 °C for 24 h alongside ball milling for 48 h. Module B has a higher material impact due to the dominance of cobalt oxide in its material architecture.

Based on toxicity impact across different variants (Fig. 12b), Module A exhibits higher toxicological impact compared to Module B, all of which is also influenced by the extremely high EEC during fabrication, although the use of tellurium, antimony, and cobalt oxide also contribute. The environmental toxicological profile of the SLT component of Module B is the lowest, due to a lower EEC. In terms of the damage to the ecosystem, resources, and human health (Fig. 12(c)), the fabrication of Module B, EEC also dominates compared to tellurium, antimony, and cobalt oxide which all have a noticeable impact as well. Overall, across all the environmental indicators considered, Module B shows a lower and better profile compared to Module A, although under the toxicological impact categories, the CCO component of Module B shows a slightly higher impact. Despite this better environmental performance of Module B, there are technical performance challenges to overcome as already highlighted in Section 2.1. As such, this is not to suggest that oxides will replace non-oxides due to their superior environmental profile given that both classes of materials thrive under different conditions for TE applications. However, the transition to oxides may be considered an environmentally intelligent move, although there are questions as to whether they can outperform heat engines, which are far more efficient for high-grade heat recovery [3].

A closer look at the energy consumption during fabrication

As highlighted in the preceding sections, EEC due to the fabrication of both Modules constitute the largest environmental impact across all indicators. In a typical primary energy demand for functional materials fabrication, the split between EEC and ME is 59%:41% (Fig. 13a and b). Assuming the electrical grid is decarbonised from 0.5 kgCO_2-eq/kWh (current emissions intensity) to 0.1 kg CO_2-eq/kWh in 2050, in line with the recommendations of the Committee on Climate Change [114], in the UK for example, the split between EEC and ME would change to 32%:68%. This increase in ME from 41% to 68% (Fig. 13a and b) suggests that, in the future, materials developers and designers may need to place more importance on strategies for the optimisation of material properties for the reduction in material usage or through intelligent specifications of materials with lower embedded impacts.

However, in the context of TE materials considered in this work, the

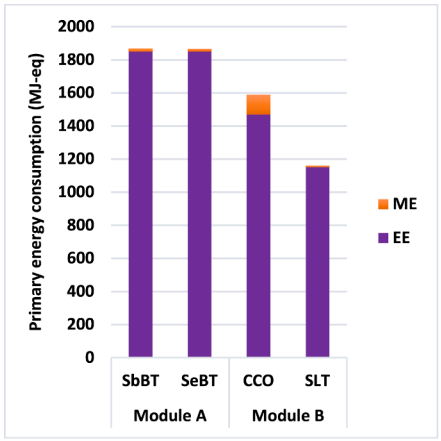

(a) Primary energy consumption

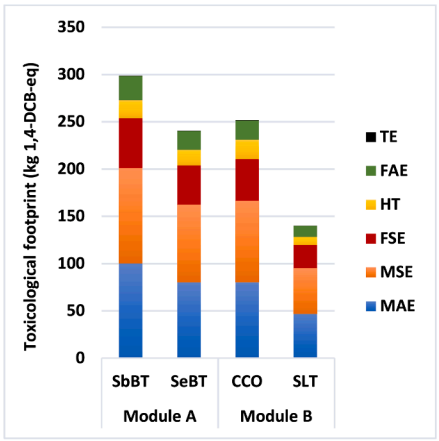

(b) Toxicological impact

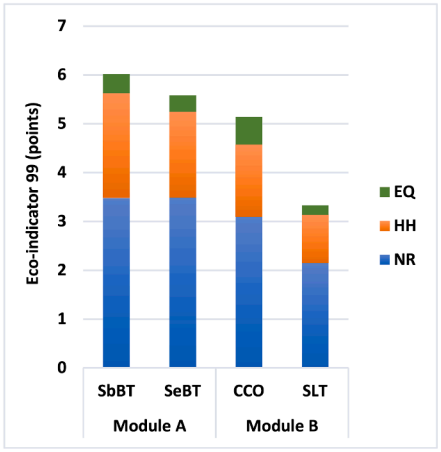

(c) Eco-indicator 99

Fig. 12. Comparison of the overall environmental profile of Modules A and B. **(a)** Primary energy demand: electrical energy (EE), materials embedded (ME). **(b)** Toxicological footprint. **(c)** Eco-indicator 99: natural resources (NR), human health (HH), ecosystem quality (EQ).

split between the impact due to EE and ME did not change considerably under the assumed decarbonisation scenarios. Although the overall impact decreased by 79% due to a fully decarbonised grid, under the baseline scenario (i.e., standard electricity mix), the split between the impact from EEC and that from ME is 98%:2%, and under a decarbonised grid, the split between EEC and ME becomes 90%:10% (Fig. 13c and d). This ratio further highlights the dominance of the EEC even after grid decarbonisation. This is a key finding and suggests that for TEs to realise their full potential, strategies towards overall reduction in the quantity of EEC during fabrication must be devised. In the current study, we analyse the emission reductions from the fabrication of TE materials by examining how energy is consumed in materials development. Understanding the flow of energy usage from the activities, processes, and materials involved in the lifecycles of these materials is pertinent to meet national and global emissions reduction targets.

If the split had been such that ME surpassed the EEC impact, it would have created huge concern because it is easier to specify intervention options for energy reduction which are readily available and better understood compared to material impact which requires optimisation of material properties. For instance, at the laboratory level, new approaches for lowering EEC have been demonstrated. Fabrication routes including microwave-assisted sintering [115], hot extrusion [116] and melt spinning [117] have been adopted to lower the EEC of non-oxide TE. Spark Plasma Sintering has also been used for Bi_2Te_3 along with several other types of materials [118]. More recently, rapid laser melting and solidification [119] have been adopted for the synthesis of selenium-doped Bi_2Te_3. EEC of oxides can also be reduced through the use of sintering aids [50] and low-temperature processing technology (e.g. cold sintering [120]). Ball milling consumes the most electrical energy in the laboratory but optimising rotational speeds and improving grinding capacity in the industry will drive down consumption whilst maintaining process control [101].

Nonetheless, it is important to highlight that in an industrial setting, these materials will be processed on a large scale and EEC will be minimised by leveraging the capacity of energy-efficient machinery and batch manufacturing processes with a greater throughput [121]. Additionally, EEC during fabrication of the TE materials can be offset by the TE energy production depending on numerous factors including TE efficiency, operating temperature, lifespan etc., as mathematically outlined in Section 4.2 and demonstrated with relevant data in the succeeding Section 5.6. Overall, when a low EEC is achieved and because the impact of the material is already established to be negligibly small, a win–win situation will thus be attained in terms of the overall environmental impact of TE. The main challenge, therefore, once EEC is diminished for large-scale applications of TE materials will be the availability/cost of the raw materials and performance.

Mathematical modelling results (performance comparison)

This section compares the performance of basic oxide-based and non-oxide-based TEG modules investigated using the power output mathematical model presented in Section 4.2, based on the assumption that the TE modules were used in an application that operates over one year. As such, the integration carried out based on Equation (24) ranges

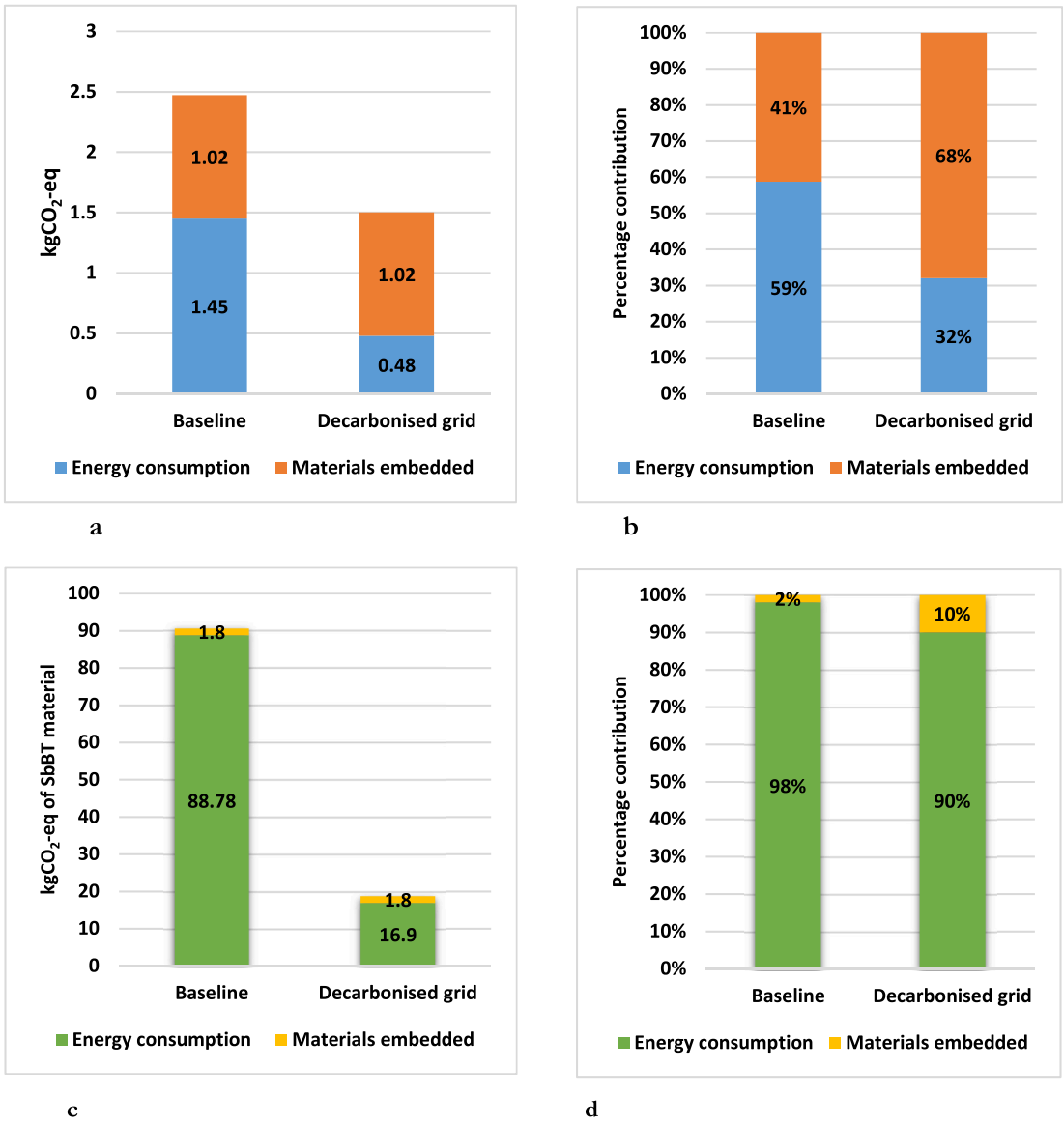

Fig. 13. Illustration of the effect of the decarbonised grid on impact from EEC due to fabrication of materials. **a)** Baseline (standard electricity mix) energy consumption during fabrication and assumed decarbonisation of the grid of a typical functional material; **b)** analysis of contributions of EEC during fabrication and materials embedded under baseline and decarbonisation assumptions, for a typical functional material; **c)** baseline EEC during fabrication and assumed decarbonisation of the grid of a thermoelectric material (e.g., SbBT) considered in this work; **d)** analysis of contributions of EEC during fabrication and materials embedded under baseline and decarbonisation assumptions. Electrical energy still dominates even under a decarbonised grid, demonstrating the importance of lowering energy consumption to realise an overall better environmental profile of TE materials.

between 0 and 365 days. Central to this performance evaluation is the set of parameters listed in Table 1. As the table indicates, we embraced the properties of Bismuth Telluride alloys, as reported in past studies [122,123], for the *p-type* and *n-type* thermoelectric elements constituting the non-oxide TEG. Similarly, for the oxide-based TEG, we gravitate towards the properties of lanthanum-doped strontium titanate and calcium cobaltite ($Ca_3Co_4O_9$) for the constituent *n-type* and *p-type* thermoelectric elements, respectively.

Premised on the above parameters, Table 2 summarized the generated power outputs of the TEGs, for a fixed value of load resistance. Listed in Table 2 is also the efficiencies of the two categories of modules. Meanwhile, the conversion efficiency of TEGs varies widely as reported in past studies, but the values reported in Table 2 are relatively within the range reported in recent surveys [12]. Fig. 14 illustrates the reduction in the energy payback period as the power output of the TEG increases. The plot combines the power output data with the total energy consumed in the production of the TEG, based on Equation (24). In all, the calculated values in Table 2 indicate a higher power output for the non-oxide TEG (472 mW) and a higher conversion efficiency of 9.4%. In contrast, the oxide-based TEG yields a power output of 356 mW with a lower conversion efficiency of 8.3%. Comparatively, these reported results are in line with those reported in earlier studies. For instance, a commercial non-oxide TEG employed by Hsiao et al. [87] in a study on automotive waste heat recovery yielded a power output of 430mW. Likewise, Wu [84] reported a power output of 265 mW for a Bismuth Telluride-based TEG under a lower temperature difference condition (100 K). It is worth pointing out that the current study is constrained to a 150 K temperature difference between the hot and cold sides of the TE unit instead of 100 K as done by Wu [84] due to the challenge with the Seebeck coefficient data for the oxide-based TE materials.

For simplicity, the calculation in this section employed the idea of an ideal waste-heat TEG in which by this, the hot junction is taken to be equivalent to a specific waste heat source whereas the cold junction temperature equals that of some ambient heat sink controlled by an

Table 1
Operating condition and parameter specifications for performance evaluations.

Parameters	Value	Unit
Hot junction temperature (T_H)	500	*K*
Cold junction temperature (T_C)	350	*K*
Load resistance [84] (R_L)	*2.33x10^{-3}*	*Ohm/couple*
Number of couple (m)	*1*	–
Oxide-based P-N elementsp-type semiconductor ($Ca_3Co_4O_9$)n-type semiconductor ($La_{0.12}Sr_{0.88})_{0.95}TiO_3$		
β_p at T_H [124]	165	$\mu V/K$
β_p at T_C [124]	146	$\mu V/K$
β_n at T_H [125]	−159	$\mu V/K$
β_n at T_C [125]	−134	$\mu V/K$
k_p [124]	0.0125	W / cm K
k_n [125]	0.0150	W / cm K
$A_n = A_p$	1	cm^2
$L_n = L_p$	1	*cm*
Non-oxide-based P-N elements n-type semiconductor: $Bi_2(Te,Se)_3$p-type semiconductor: $(Bi,Sb)_2Te_3$		
β_p at T_H [126]	220	$\mu V/K$
β_p at T_C [126]	180	$\mu V/K$
β_n at T_H [127]	−148	$\mu V/K$
β_n at T_C [127]	−135	$\mu V/K$
k_p [126]	0.014	W / cm K
k_n [127]	0.018	W / cm K
$A_n = A_p$	1	cm^2
$L_n = L_p$	1	*cm*

Table 2
Comparison of the power output, efficiency and EEC for the oxide and non-oxide-based TEGs.

TE Modules	Maximum power output	Total energy consumption	Efficiency
Non-oxide-based TEG (Module A)	472 mW	339 kWh	9.4%
Oxide-based TEG (Module B)	356 mW	240 kWh	8.3%

external cooling system [84]. Meanwhile, the Seebeck coefficients that have been used (listed in Table 1) represent average values that correspond to the hot (T_H) and cold (T_C) junctions' temperature of 500 K and 350 K, respectively. It is worth mentioning that materials research on oxide TE elements is still evolving. Hence, a notable challenge is encountered regarding the unavailability of the Seebeck coefficient for a wide range of temperature for the oxide TEG considered in this study. For this reason, the choice of T_H and T_C employed for the power calculation is contingent on the temperature range for which the Seebeck coefficient is known for the oxide TE elements. Typically, in commercially available non-oxide TE modules, the temperature of the hot and cold junctions will be expected to be somewhat lower than those specified here [128]. Nonetheless, the values of T_H and T_C used for the reported results yield an across-the-junction temperature difference (ΔT) of 150 K, which is close to the thermal condition reported for commercial TEGs deployed for the recovery of automotive exhaust waste heat [87,129].

Sensitivity analysis

Sensitivity analysis helps in the evaluation of the relationship between the input and output parameters with an LCA system, thus establishing the effect on the results when one parameter is perturbed. Essentially, sensitivity analysis helps with the identification of key parameters that have significant effects on results and those that govern the overall uncertainty of the results. In this work, sensitivity analysis was conducted using different case scenarios based on the geographical representativeness of the emissions intensity data for materials, electricity consumption and power output of the TE modules. In terms of changes in emissions intensity data of materials in the unit process exchanges outside the European market, no significant differences in impact were observed, irrespective of location (see ESI for illustration), so the resulting outputs are largely valid on a global scale.

As illustrated in Fig. 13, when the emissions intensity of electricity decreased under a decarbonisation scenario, the overall impact from EEC decreased by 79%. Further analysis was performed to determine how the manufacturing location would affect the impact of EEC during fabrication. This was carried out by comparing the emission intensity data of the electricity market (low voltage) for Great Britain with the same dataset from different countries including China, the USA, France, and Japan. The highest EEC impact was attributed to China, with the lowest impact associated with France due to the dominance of nuclear energy in its overall energy mix (see ESI for details). Finally, the role of the generated power outputs of the TE modules, for a fixed value of load resistance, on the TE energy production was demonstrated as already shown in Fig. 14. By varying the calculated power output in incremental steps, it was observed that as power output increases, the energy payback period of the TE module becomes shorter, thus demonstrating the importance of higher power output in offsetting the EEC during the fabrication of TE modules.

Limitations

It is noted that procedures for fabricating TE modules will be different from one manufacturer to another due to the application of different dopants and material substituents to improve performance properties for different applications, so LCA impact results may vary, and thus not generalisable. Specifically, there are wide variations in materials and processing techniques for non-oxide TEs, which make up the majority of TE materials. Moreover, EEC during the fabrication process is also a parameter that can vary due to its dependency on material composition. So, depending on the material constituents, certain non-oxide TE materials could consume lesser EEC compared to their oxide-based counterparts. This is also the case for oxide-based TE materials. Data inputs for the LCA model also rely on multiple assumptions in materials performance and processing parameters. Also, most of the data utilised for the power output performance of the TEGs considered were derived from the literature and experimental data from the laboratory, all of which could lead to uncertainty in results. Nonetheless, sensitivity analysis was carried out to ascertain the extent to which key parameters used in the study affected the overall results.

By leveraging new insights garnered from computationally guided parameterised models enabled by artificial intelligence (AI) methods such as machine learning (ML), alongside the proliferation of material databases, some of these limitations can be addressed in the future, facilitating better prediction lifecycle environmental impacts of TE materials with a high degree of reliability and accuracy. Although AI/ML strategies could facilitate the extent to which the comparative LCA of oxide-based vs. non-oxide TE materials can be generalised, it is highly unlikely that a generalised result will be realised due to the different compositions of materials and their processing requirements. Comparative LCA would therefore be required to be carried out on a case-by-case basis. Nonetheless, as with previous LCA work on non-oxide TE materials presented in Section 2.3, energy consumption during fabrication constitutes the biggest impact, with the only difference being the exact quantity of energy consumed, which may vary due to the different factors highlighted above. This work also concluded that EEC during fabrication also constitute the main impact for the oxide-based TE materials considered.

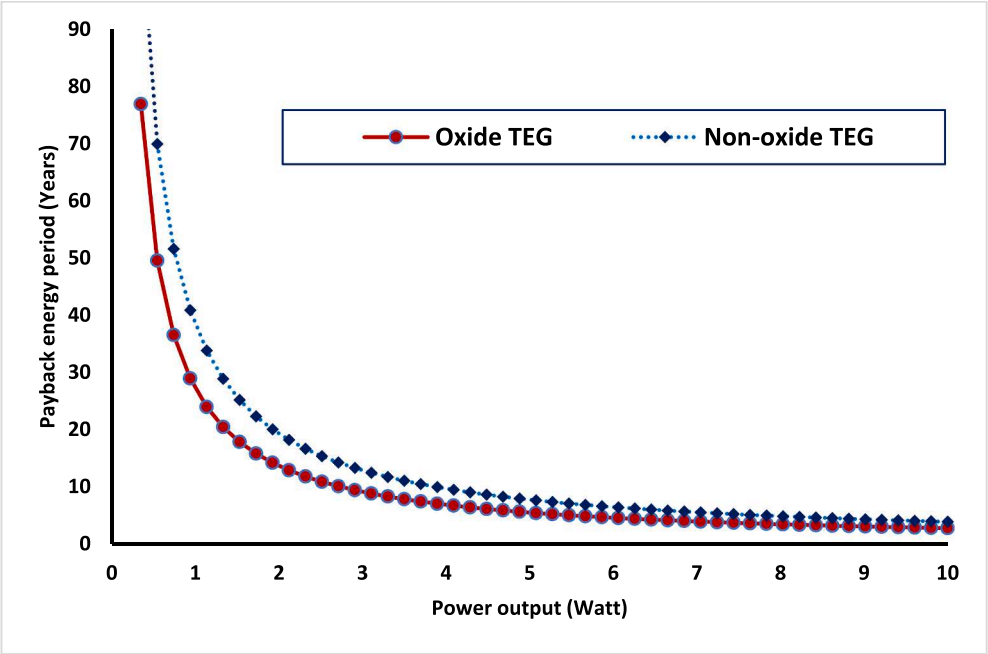

Fig. 14. Reduction in the energy payback with an increase in TEG's power output.

Conclusions

Due to high toxicity, thermal instability at high temperature, low availability, and high cost of raw materials of metallic alloys such as Bi_2Te_3 for TE applications, there has been a concerted effort to develop earth-abundant, non-toxic, environmentally friendly, and cheap TE materials, suitable for high-temperature applications. Oxide-based TEs have been touted to meet these criteria, but until now a detailed comparative LCA has not been conducted to scrutinise their environmental profile. To fill this gap, a comparative LCA of two TE modules at the laboratory level across numerous environmental indicators was carried out. Module A, which represents an example of non-oxide TE materials is based on *n*-type selenium-doped Bi_2Te_3 and *p*-type antimony-doped Bi_2Te_3. Similarly, *n*-type lanthanum-doped $SrTiO_3$ and *p*-type layered $Ca_3Co_4O_9$ constitute examples of oxide-based TE materials used in Module B. Although there are numerous non-oxides and oxides TE materials, bismuth telluride alloys were selected for Module A because they are the most widely used non-oxide TE materials due to their superior performance. For Module B, n-type lanthanum-doped strontium titanate constitutes the current leading contender and calcium cobaltite exhibits the best p-type performance, hence their selection as the representative oxide-based TE materials in this study.

Of the initial thirteen environmental impact categories initially considered, global warming, acidification, eutrophication, human toxicity and terrestrial ecotoxicity are of lesser magnitude (<2%), when the characterised results were normalised in accordance with global normalisation reference data. Noteworthy impacts include freshwater aquatic, freshwater sediment, marine aquatic, and marine sediment ecotoxicities alongside ionising radiation, malodours air and cumulative energy demand (i.e., material utilisation), and were, therefore, the indicators for which attention was paid to.

Across the ecotoxicity and environmental impact indicators considered, the material constituents of Module A, the use of tellurium and antimony exhibited noticeable environmental toxicity impacts, although very small in comparison to EEC. The rare earth elements (e.g., lanthanum oxide) contained in Module B, showed negligible environmental toxicity impact, but those from its *p-type* semiconductor thermoelements are noticeably high due to the presence of cobalt oxide. For both modules, EEC during fabrication constitutes the largest impact across all environmental indicators considered, with Module B yielding a better overall environmental profile compared to Module A due to lower EEC. Despite this better environmental performance of Module B, there are technical performance challenges to overcome. As such, this is not to suggest that the specific oxides considered in this study will replace their non-oxide equivalents due to their superior environmental profile given that both classes of materials thrive under different conditions for TE applications. However, the transition to oxides TE materials based on the specific material compositions considered in this work may be considered an environmentally intelligent move, although as highlighted in Section 5.9, this cannot be generalised until AI/ML strategies are coupled with LCA to undertake a comparative study on a variety of oxides and non-oxides.

By relying on mathematical physics modelling principles and secondary data from the literature on the TE material configurations considered, the energy production, informed by the power out of the TE modules was carried out, based on the assumption that the TE modules were used in an application that operates over one year. The model output shows that, Module A yielded a higher power output (472 mW) compared to Module B (356 mW), resulting in a shorter energy payback period (EPBP) for Module B, given the inverse relationship between power output and EPBP. Nonetheless, as the power output increases, the EPBP becomes almost identical for both modules. This underscores the significant role of thermoelectric power output in offsetting the EEC during fabrication.

Key challenges, therefore, once EEC is diminished for large-scale applications are availability and cost of raw materials as well as performance, given that both classes of materials thrive under different conditions for TE applications. For instance, non-oxide TE materials such as Bi_2Te_3 considered in this work perform better for near-room temperature applications, although other material configurations have been used for mid and high-temperature applications, however, there are technical challenges to overcome as highlighted in Section 2.1. In terms of cost, the price of tellurium, for example, somewhat negates the enhancement of ZT in Bi_2Te_3 TE [34,35]. On the other hand, oxides such as those considered in this study are more stable at high temperature and their operational temperature is typically > 400–500 °C and are therefore more suited for recovering high-grade heat, although it has been reported that TE technology may not be viable for high-grade heat

recovery because heat engines are far more efficient [3].

The LCA data presented here do not consider transitioning from laboratory to large-scale production due to the emerging nature of oxide-based TE materials. The conventional LCA methodological framework cannot be accurately used to predict the effect of scale-up of fabrication routes and is also currently incapable of future prediction of environmental impacts. Nonetheless, understanding the relevant literature describing the materials systems is essential for assessing a part of the dataset captured within the life cycle inventory. In the future, by coupling AI/ML with LCA and leveraging the proliferation of material databases, future lifecycle environmental impacts and the effect of scale-up could be predicted with a certain degree of accuracy.

Despite these challenges, we demonstrate the application of LCA early in the development of new materials when still at the laboratory or pilot scale which provides insight into how to prioritise research activities and potentially avert unintended consequences. Specifically, the LCA methodological framework presented in this work lays the foundation for evaluating the environmental impacts of any type of oxide-based TE materials to enhance their prospects for commercial applications, thus transforming their eco-friendly potential (relative to non-oxides equivalents) into reality. It is conceived that the findings from this work will assist materials scientists, planners, decision-makers, and other key stakeholders across the entire supply chain of the TE development, to look ahead and identify the consequences of products and technologies early in innovation.

CRediT authorship contribution statement

T. Ibn-Mohammed: Conceptualization, Methodology, Formal analysis, Data curation, Writing – original draft, Visualization. **S.C.L. Koh:** Supervision, Funding acquisition. **K.B. Mustapha:** Conceptualization, Methodology, Formal analysis, Data curation, Writing – original draft. **L. Smith:** Conceptualization, Methodology, Formal analysis, Data curation, Writing – original draft. **A. Acquaye:** Conceptualization, Methodology, Formal analysis, Data curation, Writing – original draft. **A.C. Iyasara:** Formal analysis, Data curation. **F. Hussain:** Formal analysis, Data curation. **N. Morley:** Supervision, Funding acquisition. **D.C. Sinclair:** Supervision, Funding acquisition. **C.A. Randall:** Supervision, Funding acquisition. **I.M. Reaney:** Supervision, Funding acquisition.

Declaration of Competing Interest

The authors declare that they have no known competing financial interests or personal relationships that could have appeared to influence the work reported in this paper.

Data availability

Data will be made available on request.

Acknowledgement.

This work was financially supported by the Engineering and Physical Sciences Research Council (EPSRC-EP/L017563/1), United Kingdom, through the University of Sheffield under the project titled: Substitution and Sustainability in Functional Materials and Devices.

Appendix A. Supplementary data

Supplementary data to this article can be found online at https://doi.org/10.1016/j.ecmx.2023.100395.

References

[1] Snyder GJ, Toberer ES. Complex thermoelectric materials. Nat Mater 2008;7(2):105–14.
[2] He J, Liu Y, Funahashi R. Oxide thermoelectrics: The challenges, progress, and outlook. J Mater Res 2011;26(15):1762–72.
[3] Vining CB. An inconvenient truth about thermoelectrics. Nat Mater 2009;8(2):83–5.
[4] US Department of Energy. Quadrennial Technology Review 2015:2015.
[5] Funahashi R, Urata S. Development of a small-size cogeneration system using thermoelectric power generation-recovery system of high-temperature waste heat by new thermoelectric oxides. Synthesiology 2008;1(2):94–100.
[6] Boston R, Schmidt WL, Lewin GD, Iyasara AC, Lu Z, Zhang H, et al. Protocols for the fabrication, characterization, and optimization of n-type thermoelectric ceramic oxides. Chem Mater 2017;29(1):265–80.
[7] Jabri M, Masoumi S, Sajadirad F, West RP, Pakdel A. Thermoelectric energy conversion in buildings. materials today. Energy 2023;32:101257.
[8] Chandel R, Chandel SS, Prasad D, Dwivedi RP. Review on thermoelectric systems for enhancing photovoltaic power generation. Sustainable Energy Technologies and Assessments. 2022;53:102585.
[9] Lan S, Li Q, Guo X, Wang S, Chen R. Fuel saving potential analysis of bifunctional vehicular waste heat recovery system using thermoelectric generator and organic Rankine cycle. Energy. 2023;263:125717.
[10] Ge M, Li Z, Zhao Y, Xuan Z, Li Y, Zhao Y. Experimental study of thermoelectric generator with different numbers of modules for waste heat recovery. Applied Energy. 2022;322:119523.
[11] Shen Z-G, Huang B, Liu X. Effect of structure parameters on the performance of an annular thermoelectric generator for automobile exhaust heat recovery. Energy Conversion and Management. 2022;256:115381.
[12] Tohidi F, Holagh SG, Chitsaz A. Thermoelectric Generators: A comprehensive review of characteristics and applications. Applied Thermal Engineering. 2022;201:117793.
[13] Koumoto K, Terasaki I, Funahashi R. Complex oxide materials for potential thermoelectric applications. MRS Bull 2006;31(3):206–10.
[14] Lee H, Han SJ, Seshadri RC, Sampath S. Thermoelectric properties of in-situ plasma spray synthesized sub-stoichiometry TiO2− x. Sci Rep 2016;6.
[15] Publisher N. Diagramatic illustration of different modes of thermoelectric effect. Nature 2015.
[16] Lu Z, Zhang H, Lei W, Sinclair DC, Reaney IM. High-figure-of-merit thermoelectric La-doped A-site-deficient SrTiO3 ceramics. Chem Mater 2016;28(3):925–35.
[17] Ravichandran J, Siemons W, Oh D-W, Kardel JT, Chari A, Heijmerikx H, et al. High-temperature thermoelectric response of double-doped SrTiO3 epitaxial films. Phys Rev B 2010;82:165126.
[18] Liu J, Wang C, Su W, Wang H, Zheng P, Li J, et al. Enhancement of thermoelectric efficiency in oxygen-deficient Sr 1− x La x TiO 3− δ ceramics. Applied Physics Letters. 2009;95:162110.
[19] DiSalvo FJ. Thermoelectric cooling and power generation. Science 1999;285(5428):703–6.
[20] Biswas K, He J, Blum ID, Wu C-I, Hogan TP, Seidman DN, et al. High-performance bulk thermoelectrics with all-scale hierarchical architectures. Nature 2012;489(7416):414–8.
[21] Hsu KF, Loo S, Guo Fu, Chen W, Dyck JS, Uher C, et al. Cubic AgPbmSbTe2+ m: bulk thermoelectric materials with high figure of merit. Science 2004;303(5659):818–21.
[22] Heremans JP, Jovovic V, Toberer ES, Saramat A, Kurosaki K, Charoenphakdee A, et al. Enhancement of thermoelectric efficiency in PbTe by distortion of the electronic density of states. Science 2008;321(5888):554–7.
[23] Wang H, Pei Y, LaLonde AD, Snyder GJ. Heavily Doped p-Type PbSe with High Thermoelectric Performance: an Alternative for PbTe. Adv Mater 2011;23(11):1366–70.
[24] Zhao L-D, Tan G, Hao S, He J, Pei Y, Chi H, et al. Ultrahigh power factor and thermoelectric performance in hole-doped single-crystal SnSe. Science 2015:aad3749..
[25] Du Z, Zhu T, Chen Yi, He J, Gao H, Jiang G, et al. Roles of interstitial Mg in improving thermoelectric properties of Sb-doped Mg 2 Si 0.4 Sn 0.6 solid solutions. J Mater Chem 2012;22(14):6838.
[26] Liu W, Tan X, Yin K, Liu H, Tang X, Shi J, et al. Convergence of conduction bands as a means of enhancing thermoelectric performance of n-type Mg 2 Si 1–x Sn x solid solutions. Phys Rev Lett 2012;108:166601.
[27] Liu X, Zhu T, Wang H, Hu L, Xie H, Jiang G, et al. Low electron scattering potentials in high performance Mg 2 Si 0.45 Sn 0.55 based thermoelectric solid solutions with band convergence. Adv Energy Mater 2013;3(9):1238–44.
[28] Shi X, Yang J, Bai S, Yang J, Wang H, Chi M, et al. On the design of high-efficiency thermoelectric clathrates through a systematic cross-substitution of framework elements. Adv Funct Mater 2010;20(5):755–63.
[29] Nolas GS, Poon J, Kanatzidis M. Recent developments in bulk thermoelectric materials. MRS Bull 2006;31(3):199–205.
[30] Sales BC, Mandrus D, Williams RK. Filled skutterudite antimonides: a new class of thermoelectric materials. Science 1996;272(5266):1325–8.
[31] Yang J, Li H, Wu T, Zhang W, Chen L, Yang J. Evaluation of half-heusler compounds as thermoelectric materials based on the calculated electrical transport properties. Adv Funct Mater 2008;18(19):2880–8.
[32] Gascoin F, Ottensmann S, Stark D, Haïle SM, Snyder GJ. Zintl phases as thermoelectric materials: tuned transport properties of the compounds CaxYb1–xZn2Sb2. Adv Funct Mater 2005;15(11):1860–4.
[33] Vaqueiro P, Powell AV. Recent developments in nanostructured materials for high-performance thermoelectrics. J Mater Chem 2010;20:9577–84.

[34] Vineis CJ, Shakouri A, Majumdar A, Kanatzidis MG. Nanostructured thermoelectrics: big efficiency gains from small features. Adv Mater 2010;22(36):3970–80.
[35] Minnich A, Dresselhaus M, Ren Z, Chen G. Bulk nanostructured thermoelectric materials: current research and future prospects. Energ Environ Sci 2009;2:466–79.
[36] Koumoto K, Wang Y, Zhang R, Kosuga A, Funahashi R. Oxide thermoelectric materials: a nanostructuring approach. Annu Rev Mat Res 2010;40(1):363–94.
[37] Ohtaki M. Recent aspects of oxide thermoelectric materials for power generation from mid-to-high temperature heat source. J Ceram Soc Jpn 2011;119(1395):770–5.
[38] Cucchiella F, D'Adamo I, Lenny Koh SC, Rosa P. Recycling of WEEEs: An economic assessment of present and future e-waste streams. Renew Sustain Energy Rev 2015;51:263–72.
[39] Hagelüken C, Lee-Shin JU, Carpentier A, Heron C. The EU circular economy and its relevance to metal recycling. Recycling 2016;1:242–53.
[40] Reck BK, Graedel TE. Challenges in Metal Recycling. Science 2012;337(6095):690–5.
[41] Awasthi AK, Li J. An overview of the potential of eco-friendly hybrid strategy for metal recycling from WEEE. Resour Conserv Recycl 2017;126:228–39.
[42] Cui J, Zhang L. Metallurgical recovery of metals from electronic waste: A review. J Hazard Mater 2008;158(2-3):228–56.
[43] Briffaerts K, Spirinckx C, Van der Linden A, Vrancken K. Waste battery treatment options: comparing their environmental performance. Waste Manag 2009;29(8):2321–31.
[44] Communication from the commission to the European Parliament, the Council, The European Economic and Social Committee and the Committee of the Regions on the 2017 list of Critical Raw Materials for the EU. 2017.
[45] Bauer D, Diamond D, Li J, Sandalow D, Telleen P, Wanner B. U.S. Department of Energy Critical Materials Strategy. 2010.
[46] Graedel TE, Barr R, Chandler C, Chase T, Choi J, Christoffersen L, et al. Methodology of metal criticality determination. Environ Sci Tech 2012;46(2):1063–70.
[47] Tanaka M, Oki T, Koyama K, Narita H, Oishi T. Chapter 255 - Recycling of Rare Earths from Scrap. In: Jean-Claude GB, Vitalij KP, editors. Handbook on the Physics and Chemistry of Rare Earths: Elsevier; 2013. p. 159–211.
[48] Binnemans K, Jones PT, Blanpain B, Van Gerven T, Yang Y, Walton A, et al. Recycling of rare earths: a critical review. J Clean Prod 2013;51:1–22.
[49] Rocchetti L, Vegliò F, Kopacek B, Beolchini F. Environmental impact assessment of hydrometallurgical processes for metal recovery from WEEE residues using a portable prototype plant. Environ Sci Tech 2013;47:1581–8.
[50] Ibn-Mohammed T, Koh SCL, Reaney IM, Acquaye A, Wang D, Taylor S, et al. Integrated Hybrid Life Cycle Assessment and Supply Chain Environmental Profile Evaluations of Lead-based (Lead Zirconate Titanate) versus Lead-free (Potassium Sodium Niobate) Piezoelectric Ceramics. Energ Environ Sci 2016;9(11):3495–520.
[51] Graedel TE, Allwood J, Birat J-P, Buchert M, Hagelüken C, Reck BK, et al. What Do We Know About Metal Recycling Rates? J Ind Ecol 2011;15(3):355–66.
[52] European Commission D-GJRCGAB, Darina Blagoeva, Jo Dewulf, Cristina Torres de Matos, Claudia Baranzelli, Constantin Ciupagea, Patrícia Dias, Yildirim Kayam, Cynthia E.L. Latunussa, Lucia Mancini, Simone Manfredi, Alain Marmier, Fabrice Mathieux, Viorel Nita, Philip Nuss, Claudiu Pavel, Laura Talens Peirò, Evangelos Tzimas, Beatriz Vidal-Legaz and David Pennington. Mthodology for establishing the EU list of critical raw materials; Raw materials Guidelines. 2017.
[53] Sagar AD, Frosch RA. A perspective on industrial ecology and its application to a metals-industry ecosystem. J Clean Prod 1997;5(1-2):39–45.
[54] EU Non-critial materials.
[55] USGS Mineral Commodity Summaries.
[56] Takeda O, Okabe TH. Current Status of Titanium Recycling and Related Technologies. JOM 2019;71(6):1981–90.
[57] The Global Goals for Sustainable Development.
[58] Report on Critical Raw Materials for the EU. In: Commission E, editor.2014.
[59] Royal Society of Chemistry.
[60] Soleimani Z, Zoras S, Ceranic B, Shahzad S, Cui Y. The cradle to gate life-cycle assessment of thermoelectric materials: A comparison of inorganic, organic and hybrid types. Sustainable Energy Technologies and Assessments. 2021;44:101073.
[61] Patyk A. Thermoelectric generators for efficiency improvement of power generation by motor generators–environmental and economic perspectives. Appl Energy 2013;102:1448–57.
[62] Patyk A. Thermoelectrics: impacts on the environment and sustainability. J Electron Mater 2010;39(9):2023–8.
[63] Kishita Y, Ohishi Y, Uwasu M, Kuroda M, Takeda H, Hara K. Evaluating the life cycle CO2 emissions and costs of thermoelectric generators for passenger automobiles: a scenario analysis. J Clean Prod 2016;126:607–19.
[64] Kishita Y, Uwasu M, Takeda H, Hara K, Ohishi Y, Kuroda M. Assessing the greenhouse gas emissions and cost of thermoelectric generators for passenger automobiles: a life cycle perspective. International Design Engineering Technical Conferences and Computers and Information in Engineering Conference: American Society of Mechanical Engineers; 2014. p. V004T06A30.
[65] Iyer RK, Pilla S. Environmental profile of thermoelectrics for applications with continuous waste heat generation via life cycle assessment. Science of The Total Environment. 2021;752:141674.
[66] Kawajiri K, Kishita Y, Shinohara Y. Life cycle assessment of thermoelectric generators (TEGs) in an automobile application. Sustainability 2021;13:13630.
[67] Irshad K, Habib K, Algarni S, Saha BB, Jamil B. Sizing and life-cycle assessment of building integrated thermoelectric air cooling and photovoltaic wall system. Appl Therm Eng 2019;154:302–14.
[68] Sergienko O, Bulat L, Kopyltsova S, Shestopalova A, Guzhva M, Vinogradov A. Environmental aspects of thermoelectric cooling. Journal of Thermoelectricity 2010:5–10.
[69] Søndergaard RR, Hösel M, Espinosa N, Jørgensen M, Krebs FC. Practical evaluation of organic polymer thermoelectrics by large-area R2R processing on flexible substrates. Energy Sci Eng 2013;1(2):81–8.
[70] Bhame SD, Pravarthana D, Prellier W, Noudem JG. Enhanced thermoelectric performance in spark plasma textured bulk n-type BiTe2. 7Se0. 3 and p-type Bi0. 5Sb1. 5Te3. Applied Physics Letters. 2013;102:211901.
[71] Tang Z, Hu L, Zhu T, Liu X, Zhao X. High performance n-type bismuth telluride based alloys for mid-temperature power generation. J Mater Chem C 2015;3(40):10597–603.
[72] Hu L, Gao H, Liu X, Xie H, Shen J, Zhu T, et al. Enhancement in thermoelectric performance of bismuth telluride based alloys by multi-scale microstructural effects. J Mater Chem 2012;22(32):16484.
[73] Hu L, Zhu T, Liu X, Zhao X. Point Defect Engineering of High-Performance Bismuth-Telluride-Based Thermoelectric Materials. Adv Funct Mater 2014;24(33):5211–8.
[74] Sivanagaraju S. Generation and utilization of electrical energy. Pearson Education India; 2010.
[75] Kenfaui D, Bonnefont G, Chateigner D, Fantozzi G, Gomina M, Noudem JG. Ca3Co4O9 ceramics consolidated by SPS process: Optimisation of mechanical and thermoelectric properties. Mater Res Bull 2010;45(9):1240–9.
[76] Ibn-Mohammed T, Greenough R, Taylor S, Ozawa-Meida L, Acquaye A. Operational vs. embodied emissions in buildings—a review of current trends. Energ Buildings 2013;66:232–45.
[77] Acquaye AA, Wiedmann T, Feng K, Crawford RH, Barrett J, Kuylenstierna J, et al. Identification of 'carbon hot-spots' and quantification of GHG intensities in the biodiesel supply chain using hybrid LCA and structural path analysis. Environ Sci Tech 2011;45(6):2471–8.
[78] Collado-Ruiz D, Ostad-Ahmad-Ghorabi H. Comparing LCA results out of competing products: developing reference ranges from a product family approach. J Clean Prod 2010;18(4):355–64.
[79] Ecoinvent. Ecoinvent database. 2020.
[80] Geisler G, Hofstetter TB, Hungerbühler K. Production of fine and speciality chemicals: procedure for the estimation of LCIs. Int J LCA 2004;9(2):101–13.
[81] Goedkoop M, Effting S, Collignon M. The Eco-indicator 99: A damage oriented method for life-cycle impact assessment: Manual for designers: PRé Consultants; 2000.
[82] Kim J, Yang Yi, Bae J, Suh S. The importance of normalization references in interpreting life cycle assessment results. J Ind Ecol 2013;17(3):385–95.
[83] Frischknecht R, Jungbluth N, Althaus H, Bauer C, Doka G, Dones R, et al. Implementation of life cycle impact assessment methods. 2007.
[84] Wu C. Analysis of waste-heat thermoelectric power generators. Appl Therm Eng 1996;16(1):63–9.
[85] Yu J, Zhao H. A numerical model for thermoelectric generator with the parallel-plate heat exchanger. J Power Sources 2007;172(1):428–34.
[86] Stevens JW. Optimal design of small ΔT thermoelectric generation systems. Energ Conver Manage 2001;42(6):709–20.
[87] Hsiao YY, Chang WC, Chen SL. A mathematic model of thermoelectric module with applications on waste heat recovery from automobile engine. Energy 2010;35(3):1447–54.
[88] Bellos E, Tzivanidis C. Energy and financial analysis of a solar driven thermoelectric generator. J Clean Prod 2020;264:121534.
[89] Feidt M. Finite Physical Dimensions Optimal Thermodynamics 1. Fundamentals: Elsevier; 2017.
[90] Wang Y, Dai C, Wang S. Theoretical analysis of a thermoelectric generator using exhaust gas of vehicles as heat source. Appl Energy 2013;112:1171–80.
[91] Hodes M. Optimal pellet geometries for thermoelectric power generation. IEEE Trans Compon Packag Technol 2010;33(2):307–18.
[92] Hans Wedepohl K. The composition of the continental crust. Geochim Cosmochim Acta 1995;59(7):1217–32.
[93] Peiró LT, Méndez GV, Ayres RU. Material flow analysis of scarce metals: sources, functions, end-uses and aspects for future supply. Environ Sci Tech 2013;47(6):2939–47.
[94] Makuei FM, Senanayake G. Extraction of tellurium from lead and copper bearing feed materials and interim metallurgical products–a short review. Miner Eng 2018;115:79–87.
[95] Harada T, Takahashi Y. Origin of the difference in the distribution behavior of tellurium and selenium in a soil–water system. Geochim Cosmochim Acta 2008;72(5):1281–94.
[96] Ba LA, Döring M, Jamier V, Jacob C. Tellurium: an element with great biological potency and potential. Org Biomol Chem 2010;8:4203–16.
[97] Belzile N, Chen Y-W. Tellurium in the environment: A critical review focused on natural waters, soils, sediments and airborne particles. Appl Geochem 2015;63:83–92.
[98] Gerhardsson L. Tellurium. Handbook on the Toxicology of Metals (Fourth Edition): Elsevier; 2015. p. 1217–28.
[99] Filella M, Williams PA, Belzile N. Antimony in the environment: knowns and unknowns. Environ Chem 2009;6:95–105.
[100] Cooper RossG, Harrison AdrianP. The exposure to and health effects of antimony. Indian journal of occupational and environmental medicine 2009;13(1):3.

[101] Ibn-Mohammed T, Reaney IM, Koh SCL, Acquaye A, Sinclair DC, Randall CA, et al. Life cycle assessment and environmental profile evaluation of lead-free piezoelectrics in comparison with lead zirconate titanate. J Eur Ceram Soc 2018; 38(15):4922–38.
[102] Reuter M, Hudson C, Van Schaik A, Heiskanen K, Meskers C, Hagelüken C. Metal recycling: opportunities, limits, infrastructure. A report of the working group on the global metal flows to the international resource panel. 2013.
[103] European Union Commission. Critical raw materials for the EU. Report of the Ad-hoc Working Group on defining critical raw materials. 2010.
[104] Haque N, Hughes A, Lim S, Vernon C. Rare earth elements: Overview of mining, mineralogy, uses, sustainability and environmental impact. Resources 2014;3: 614–35.
[105] Alonso E, Sherman AM, Wallington TJ, Everson MP, Field FR, Roth R, et al. Evaluating rare earth element availability: A case with revolutionary demand from clean technologies. Environ Sci Tech 2012;46(6):3406–14.
[106] Weng ZH, Jowitt SM, Mudd GM, Haque N. Assessing rare earth element mineral deposit types and links to environmental impacts. Appl Earth Sci 2013;122(2): 83–96.
[107] Weng Z, Haque N, Mudd GM, Jowitt SM. Assessing the energy requirements and global warming potential of the production of rare earth elements. J Clean Prod 2016;139:1282–97.
[108] Bogart JA, Cole BE, Boreen MA, Lippincott CA, Manor BC, Carroll PJ, et al. Accomplishing simple, solubility-based separations of rare earth elements with complexes bearing size-sensitive molecular apertures. Proc Natl Acad Sci USA 2016;113(52):14887–92.
[109] Domingo JL. Cobalt in the environment and its toxicological implications. Rev Environ Contam Toxicol 1989;105–32.
[110] Fordyce FM. Selenium deficiency and toxicity in the environment. Essentials of medical geology: Springer; 2013. p. 375–416.
[111] Tkaczyk A, Bartl A, Amato A, Lapkovskis V, Petranikova M. Sustainability evaluation of essential critical raw materials: cobalt, niobium, tungsten and rare earth elements. Journal of Physics D: Applied Physics. 2018;51:203001.
[112] Pazik PM, Chmielewski T, Glass HJ, Kowalczuk PB, Kowalczuk PB, Drzymala J. World production and possible recovery of cobalt from the Kupferschiefer stratiform copper ore. E3S web of conferences: EDP Sciences 2016;8:01063.
[113] Farjana SH, Huda N, Mahmud MAP. Life cycle assessment of cobalt extraction process. J Sustainable Min 2019;18(3):150–61.
[114] Committee for Climate Change. Building a low-carbon economy - the UK's contribution to tackling climate change. 2008.
[115] Delaizir G, Bernard-Granger G, Monnier J, Grodzki R, Kim-Hak O, Szkutnik P-D, et al. A comparative study of Spark Plasma Sintering (SPS), Hot Isostatic Pressing (HIP) and microwaves sintering techniques on p-type Bi2Te3 thermoelectric properties. Mater Res Bull 2012;47(8):1954–60.
[116] André C, Vasilevskiy D, Turenne S, Masut RA. Extruded bismuth-telluride-based n-type alloys for waste heat thermoelectric recovery applications. J Electron Mater 2009;38(7):1061–7.
[117] Xie W, Tang X, Yan Y, Zhang Q, Tritt TM. Unique nanostructures and enhanced thermoelectric performance of melt-spun BiSbTe alloys. Applied Physics Letters. 2009;94:102111.
[118] Molénat G, Thomas M, Galy J, Couret A. Application of spark plasma sintering to titanium aluminide alloys. Adv Eng Mater 2007;9(8):667–9.
[119] Mao Yu, Yan Y, Wu K, Xie H, Xiu Z, Yang J, et al. Non-equilibrium synthesis and characterization of n-type Bi 2 Te 2.7 Se 0.3 thermoelectric material prepared by rapid laser melting and solidification. RSC. Advances 2017;7(35):21439–45.
[120] Guo H, Baker A, Guo J, Randall CA, Johnson D. Cold Sintering Process: A Novel Technique for Low-Temperature Ceramic Processing of Ferroelectrics. J Am Ceram Soc 2016;99(11):3489–507.
[121] Fang K, Uhan N, Zhao Fu, Sutherland JW. A new approach to scheduling in manufacturing for power consumption and carbon footprint reduction. J Manuf Syst 2011;30(4):234–40.
[122] Jiang J, Chen L, Bai S, Yao Q, Wang Q. Fabrication and thermoelectric performance of textured n-type Bi2 (Te, Se) 3 by spark plasma sintering. Mater Sci Eng B 2005;117(3):334–8.
[123] Jiang J, Chen L, Bai S, Yao Q, Wang Q. Thermoelectric properties of textured p-type (Bi, Sb)2Te3 fabricated by spark plasma sintering. Scr Mater 2005;52(5): 347–51.
[124] Wu N. Development and processing of p-type oxide thermoelectric materials. 2014.
[125] Singh SP, Kanas N, Desissa TD, Johnsson M, Einarsrud M-A, Norby T, et al. Thermoelectric properties of A-site deficient La-doped SrTiO3 at 100–900 °C under reducing conditions. J Eur Ceram Soc 2020;40(2):401–7.
[126] Shin HS, Ha HP, Hyun DB, Shim JD, Lee DH. Thermoelectric properties of 25% Bi2Te3-75%Sb2Te3 solid solution prepared by hot-pressing method. J Phys Chem Solid 1997;58(4):671–8.
[127] Jiang J, Chen L, Bai S, Yao Q, Wang Q. Fabrication and thermoelectric performance of textured n-type Bi2(Te, Se)3 by spark plasma sintering. Mater Sci Eng B 2005;117(3):334–8.
[128] How Thermoelectric Power Generation Works. Thermal Electronics Corp.; 2022.
[129] He W, Wang S, Zhang X, Li Y, Lu C. Optimization design method of thermoelectric generator based on exhaust gas parameters for recovery of engine waste heat. Energy 2015;91:1–9.